

# CausalSim: Unbiased Trace-Driven Network Simulation

Abdullah Alomar\*  
MIT  
aalomar@mit.edu

Pouya Hamadani\*  
MIT  
pouyah@mit.edu

Arash Nasr-Esfahany\*  
MIT  
arashne@mit.edu

Anish Agarwal  
MIT  
anish90@mit.edu

Mohammad Alizadeh  
MIT  
alizadeh@mit.edu

Devavrat Shah  
MIT  
devavrat@mit.edu

## ABSTRACT

Evaluating the real-world performance of network protocols is challenging. Randomized control trials (RCT) are expensive and inaccessible to most, while simulators fail to capture complex behaviors in real networks. We present CausalSim, a trace-driven counterfactual simulator for network protocols that addresses this challenge. Counterfactual simulation aims to predict what would happen using different protocols under the same conditions as a given trace. This is complicated due to the bias introduced by the protocols used during trace collection. CausalSim uses traces from an initial RCT under a set of protocols to learn a *causal* network model, effectively removing the biases present in the data. Key to CausalSim is mapping the task of counterfactual simulation to that of tensor completion with extremely sparse observations. Through an adversarial neural network training technique that exploits distributional invariances that are present in training data coming from an RCT, CausalSim enables a novel tensor completion method despite the sparsity of observations. Our extensive evaluation of CausalSim on both real and synthetic datasets and two use cases, including more than nine months of real data from the Puffer video streaming system, shows that it provides accurate counterfactual predictions, reducing prediction error by 44% and 53% on average compared to expert-designed and supervised learning baselines.

## 1 INTRODUCTION

*Causa Latet Vis Est Notissima – The cause is hidden, but the result is known. (Ovid: Metamorphoses IV, 287)*

Evaluating the real-world performance of network protocols is challenging. The gold standard is to run randomized control trials (RCT). However, RCTs are time consuming, risk disruptions or SLA violations [37], and require significant infrastructure that is available only to large network operators. The research community typically resorts to network simulators (e.g., NS3 [26]) or trace-driven simulation (or emulation) to assess new ideas. However, network simulators are

notoriously unreliable in capturing real-world behavior [21] and they require detailed knowledge of network characteristics (e.g., topology, traffic patterns, etc.). On the other hand, trace-driven simulation, as we will see in this paper, is fraught with challenges due to data quality and bias issues [12, 33, 65].

This paper investigates the problem of learning a model to perform *counterfactual* simulation of network protocols using offline historical data. Given a trace describing the system trajectory for one protocol, our goal is to produce the hypothetical system trajectory that would have occurred if we had used a different protocol under the same conditions. Such a model, if accurate, would allow network operators to rapidly evaluate new ideas under real conditions without deploying them on their network. By contrast, today even those operators who have the ability to perform RCTs, can afford to evaluate only a small fraction of proposals. Moreover, full-trajectory simulation provides more insights than merely collecting performance metrics for a protocol in the wild. Designers can inspect and compare the actions of different protocols under the exact same conditions to understand their behavior and diagnose problems. Finally, if accurate counterfactual simulators based on real networks existed, operators could share them with the research community, enabling those without access to large networks to benchmark their ideas.

While obviously appealing, counterfactual trace-driven simulation is difficult. As we discuss in depth in §2, the challenge lies in biases introduced into the observed data by the protocols used during data collection. Consider, for example, a trace of the execution of an adaptive bitrate (ABR) algorithm [30, 46, 58, 65, 67] during a video streaming session. Observed quantities, such as the throughput achieved when the player downloads a video chunk, are caused by certain *latent* properties of the network path (e.g., the underlying bottleneck capacity, the number and type of competing flows, etc.), as well as the particular choices made by the ABR algorithm (the bitrates chosen for each chunk). The observed data reflects the combined effect of these two *causes*. But to simulate a new algorithm, we need to identify the underlying latent factors (i.e. the unobserved cause) and the causal relationships that lead to the

\*Equal Contribution

observations. Only then can we answer counterfactual questions like “what would have happened had the ABR selected a higher bitrate at this point in a video streaming session?”

We present CausalSim, a framework for learning unbiased trace-driven counterfactual simulation models for network protocols. CausalSim can be applied in a wide range of networking problems, such as ABR algorithms, congestion control, load balancing, and more. CausalSim starts with traces collected using an initial RCT under a set of protocols. It uses this data to learn a causal model of the underlying network dynamics. CausalSim’s model can then be used to simulate any protocol (including new ones that were not in the RCT) on any of the traces collected during the RCT. Therefore, while CausalSim requires an RCT for training, it greatly extends the utility of this initial RCT by enabling the evaluation of new *unseen* protocols. Periodically or whenever an operator believes the underlying path characteristics have changed significantly, they can collect fresh data using an RCT (again, with the same fixed set of protocols) to retrain CausalSim.

CausalSim simulates a new protocol in two steps. First, it estimates the latent factors at every time step of each trace based on the observed data. Then, it uses the estimated latent factors to predict the alternate evolution of actions and observed variables, under the same conditions for the new protocol. This two-step process effectively removes the bias introduced by the protocol that was used to collect the trace, enabling accurate counterfactual simulation.

CausalSim’s design begins with the observation that counterfactual estimation can be viewed as a matrix (or tensor) completion problem [6, 11]. Consider a matrix  $M$  of observations (it is a tensor if observations are higher dimensional), with rows corresponding to possible protocol actions and columns corresponding to different time steps in the trace data. For each column, the entry for one action is “revealed”; all other entries are missing. Counterfactual estimation can be viewed as recovering the missing entries. This is of course hopeless in general, but a significant body of work has shown that recovery is possible under certain assumptions about the matrix and the pattern of missing data. Roughly speaking, the typical assumptions for recovery to be possible are that the matrix has low rank, the entries revealed are chosen at random, and that enough entries are revealed. Low-rank structure is prevalent in many real-world problems [64] and has also been observed in network measurement data [13, 38, 39, 55]. But unfortunately the other two assumptions do not hold in our problem. As we detail in §4.1, one observed entry per column is below the information-theoretic bound for low-rank matrix completion (even for rank  $r = 1$ ). Moreover, not only are the entries revealed in our problem not random, they depend on other entries of the matrix, since the actions are being taken by protocols based on observed variables.

CausalSim exploits a novel form of additional problem structure to overcome these challenges. First, it assumes a network model (§3) where the latent factors are *exogenous* properties of a network path, beyond the impact of a particular user’s actions. For example, in ABR, the bottleneck link speed on a network path is not affected by a user’s ABR policy, whereas ABR decisions do impact what that user *observes* (e.g., the achieved throughput). Second, CausalSim uses a basic feature of training data collected via an RCT. Since an RCT assigns protocols to users (and thus network paths) at random, we expect the distribution of the exogenous latent network properties to be the same for the traces obtained using different protocols. We show that this “policy invariance” of the latent variable distribution is sufficient to recover low-rank matrices in our setup (§4.2), and we operationalize this idea in a practical learning algorithm that exploits the invariance using an adversarial neural network training technique (§5).

We evaluate CausalSim on two use cases, ABR and server load balancing, with both real-world and synthetic datasets. Our main findings are:

- (1) Evaluation of CausalSim on more than nine months of real data from the Puffer [65] video streaming system shows 44% and 53% reduction in average counterfactual prediction error with respect to expert-designed and standard supervised learning baselines, respectively.
- (2) Using a synthetic (simulated) network environment, we find that a Reinforcement Learning (RL) ABR policy [46] trained on a CausalSim model of the environment performs similarly to a policy trained directly through interaction with the environment.<sup>1</sup> Compared to the baseline simulators, training on CausalSim lead to a 200 kbps boost in attained bitrate with a small increase in rebuffering, resulting in a 5.8% better QoE metric (and 26% in populations where not accounting for latent factors leads to a more noticeable bias). Policies trained on the baseline simulator underutilize the network, performing even worse than the non-learning policies (e.g., MPC [67]) used to collect the trace data.
- (3) Evaluation of CausalSim on a synthetic load balancing dataset shows that its representation of the latent factors has extremely high accuracy i.e. Pearson Correlation Coefficient (PCC) of 0.99 with the latent job size value, enabling accurate counterfactual simulation.

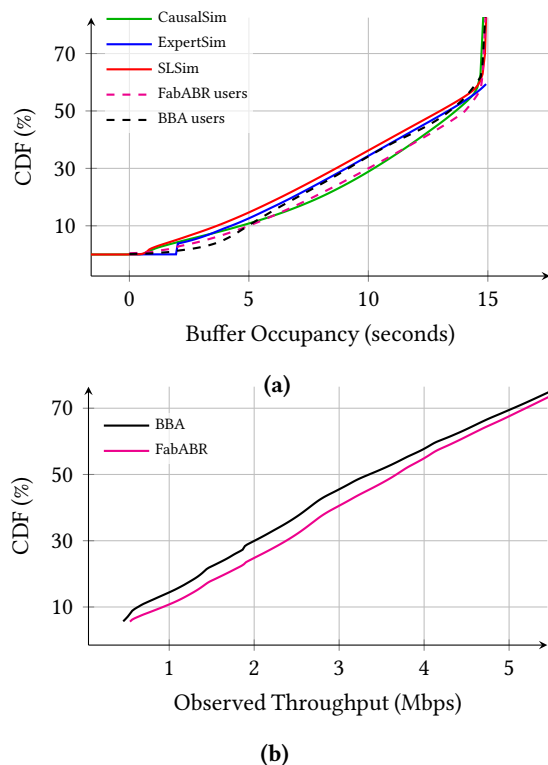


**Figure 1: Top: CausalSim is accurate in predicting buffer level distribution of FabABR users, while baseline simulators’ predictions are similar to BBA users. Bottom: Distribution of achieved throughput is different in BBA and FabABR users.**

## 2 MOTIVATION

Suppose a graduate student designs a new Adaptive Bit Rate (ABR) algorithm, which selects a bitrate amongst several options for each video chunk (e.g., 2 seconds of video) based on network conditions. The student calls the algorithm *FabABR* (Fabulous ABR) and claims that it leads to 50% lower rebuffering than Buffer-Based Algorithm (BBA) [30], according to simulations on a set of network traces. A video service provider becomes interested in FabABR and wishes to evaluate it on its own network. The standard approach to do so would be to run a Randomized Control Trial (RCT). However, an RCT is time-consuming and has potential undesirable side effects (some users getting poorer experience), and hence it is not feasible to run an RCT everytime a new proposal is made. This naturally raises the following questions: (i) Is it possible to predict the performance of FabABR using historical observational data? (ii) Could a service provider use historical data to build

<sup>1</sup>We use a simulated environment for these experiments due to time constraints. The Puffer [65] paper estimates that it takes about 8 months of data collection to make a statistically significant comparison of ABR policies in the wild due to high variability across network paths (see §6.2 for details).

a realistic simulation model that would enable researchers to evaluate their ideas without direct access to the real network?

### 2.1 The Problem with Trace-Driven Network Simulation

This section describes two strawman approaches to address the tasks above using trace-driven network modeling and simulation. For concreteness, we evaluate these approaches with more than nine months of data from Puffer, a recently deployed system for experimenting with video streaming techniques [65]. Through this study, we show the pitfalls of using standard trace-driven simulation techniques to evaluate network protocols.

Puffer collects data from a continual RCT switching between several ABR algorithms. In the period of interest (1 August 2020 – 15 May 2021), the tested algorithms include BBA [30], two versions of BOLA-BASIC [58]<sup>2</sup>, and two versions of an algorithm called Fugu developed by the Puffer authors. The dataset we use includes more than 62 million chunk downloads of more than 32 thousand streaming sessions, totaling four years of streamed videos. To evaluate a new ABR algorithm, we may be interested in various performance measurements, e.g. buffer occupancy, rebuffering rate, chunk download time, chosen chunk sizes, etc. For simplicity, we focus only on predicting the distribution of playback buffer occupancy. The buffer dynamics capture the core behavior of ABR algorithms and serve as a good proxy for other metrics of interest like rebuffering.

The Puffer dataset<sup>3</sup> contains logs of chosen chunk sizes, available chunk sizes, achieved chunk download throughputs, and playback buffer levels. We let BOLA-BASIC v1 play the role of the new “FabABR” algorithm that we wish to evaluate. So our task is: *predict the distribution of buffer level for the users assigned to BOLA-BASIC v1 (henceforth called FabABR) in the Puffer dataset, using only the data from the other algorithms.*

Before proceeding, it is important to make a subtle point. Our ultimate goal is more ambitious than the above task suggests. By trace-driven simulation, we mean predicting the *entire trajectory* of the system (e.g., buffer, bitrates, etc.) for one algorithm in *the same network conditions* that were present when a trace was collected using a different algorithm. Full trajectory simulation provides more insight than merely evaluating a policy’s performance. It allows a designer to inspect the algorithm’s actions in detail and diagnose/debug problems. When simulating algorithm *B* based on a trace collected

<sup>2</sup>BOLA-BASIC v1 and v2 are variations on BOLA-BASIC adjusted to target the SSIM quality metric instead of bitrate [49]. They pursue different objective functions and use different principles for hyperparameter adjustment.

<sup>3</sup>We select logs, available on the puffer website, with a minimum length of 500 chunks ( $\approx 17$  minutes) and average observed throughputs below 7 Mbps.

using algorithm  $A$ , we will refer to  $A$  as the “source” algorithm (or policy) and to  $B$  as the “target” algorithm.

Unfortunately, it is not possible to evaluate the accuracy of full trajectory simulation in practice, because we don’t have ground truth for the target algorithm under the same exact network conditions that were present when running the source algorithm. Therefore, as a proxy, we validate predictions about distributional properties of the target algorithm, such as the CDF of buffer occupancy for FabABR which we can obtain from the Puffer data. In our evaluation, we also use synthetic network environments where we can obtain ground-truth trajectories for any algorithm to bridge this gap (see §D.3).

**2.1.1 Simulation via Expert Modeling (ExpertSim).** As our first strawman, we build a simple trace-driven simulator (ExpertSim) using our knowledge of how an ABR system works. ExpertSim models the playback buffer dynamics for each *step*, where a step corresponds to one ABR decision and the download of a single video chunk. Let  $\hat{c}_t$  be the throughput achieved in step  $t$  (for the  $t^{\text{th}}$  chunk) of a particular video streaming session using, say, the BBA algorithm. To simulate FabABR for the same user, ExpertSim assumes that the user would achieve the same throughput  $\hat{c}_t$  in each step under the FabABR algorithm as well. In other words, it assumes that the different actions of the ABR algorithms (BBA vs. FabABR) do not affect the observed network throughput. Under this assumption, ExpertSim models the evolution of the video playback buffer for FabABR as follows. Let  $b_t$  be the buffer level at the beginning of step  $t$  (before the download of chunk  $t$ ),  $r_t$  be the bitrate chosen by FabABR in step  $t$ , and  $s_t$  be the size of the  $t^{\text{th}}$  chunk implied by the bitrate chosen by FabABR. Then the buffer at the end of step  $t$  is derived as:  $b_{t+1} = \max(0, b_t - s_t / \hat{c}_t) + T$ , where  $T$  is the chunk duration.<sup>4</sup> Although simple, the assumption that throughput is an “exogenous” property of a network path is common in modelling ABR protocols. For example, both FastMPC [67] and FESTIVE [34] assume that the observed throughput does not depend on the chosen bitrate.

Figure 1a shows the true distribution of buffer level for BBA and FabABR (BOLA-BASIC v1) users in the Puffer dataset (the two dashed lines), as well as the distribution *predicted* by running FabABR on the traces collected from BBA users using ExpertSim (solid blue line). We see that the predictions are inaccurate: the buffer distribution generated by ExpertSim closely follows the buffer distribution of BBA users (the “source” algorithm) and fails to match the buffer distribution of FabABR users (the “target” algorithm).

**2.1.2 Simulation via Supervised Learning (SLSim).** Perhaps the simple model of buffer dynamics in ExpertSim does not

accurately reflect the actual system behavior. As a next attempt, we turn to machine learning and try to learn the system dynamics from data. Specifically, we use supervised learning to train a neural network that models the step-wise dynamics of the system. This fully connected neural network includes 2 hidden layers, each with 128 ReLU activated neurons. For each timestep  $t$ , the neural network takes as input the buffer level before download of  $t$ -th chunk  $b_t$ , the achieved throughput  $\hat{c}_t$  for chunk  $t$ , and the chunk size  $s_t$  (which depends on the bitrate chosen by ABR). The neural network outputs the buffer level after the download of  $t$ -th chunk  $b_{t+1}$ . We train the neural network to minimize the mean squared error of the predictions (L2 loss) on our dataset. To avoid information leaking, we exclude the logs for FabABR from the training data.

Figure 1a shows the predicted buffer level distribution via this approach (SLSim) for FabABR. As with ExpertSim, we use the traces collected from BBA users as the source algorithm. The results are similar to ExpertSim; once again, the predicted buffer distribution is closer to that of BBA than FabABR.

**2.1.3 What Went Wrong?** To understand the limitations of ExpertSim and SLSim, we plot the distribution of achieved per-chunk throughput for users assigned to BBA and FabABR in Figure 1b. Since policy assignment is completely random, we would expect inherent network path properties such as bottleneck link capacity to have the same distribution for users assigned to different ABR policies. However, such an invariance should not be expected for achieved throughput, because even on the same path different ABR algorithms could achieve different throughput. For example, since congestion control protocols take time to discover available bandwidth (e.g., in slow start) or converge to their fair share rate when competing against other flows, an ABR algorithm that tends to choose lower bitrates (and hence download less data per chunk) may achieve less throughput than an ABR algorithm that picks higher bitrates [29]. We can see this behavior in the Puffer dataset. The achieved throughput for BBA and FabABR is clearly different in Figure 1b.

Indeed, the fundamental flaw in both ExpertSim and SLSim is that they view the achieved throughput observed in a trace as an exogenous property of that network path, unaffected by ABR. However, the throughput achieved when downloading a video chunk is impacted by the actions taken by the ABR policy. This “bias”, induced by the actions of a network protocol on observed behavior, needs to be carefully corrected for accurate trace-driven simulation.

## 2.2 Causal Inference to the Rescue!

If the traces provided the *underlying network capacity* when each chunk was downloaded (rather than only the achieved throughput), our problem would be simple. First, we would learn the relationship between network capacity and achieved

<sup>4</sup>The complete buffer dynamic equation is slightly more complex, to handle cases with full buffers. Refer to §D.1 in the appendix for further clarification.

throughput for different ABR actions using our data. Then, to simulate FabABR for a given trace, we would start with the network capacity at each step of the trace and predict the achieved throughput taking into account the bitrate chosen by FabABR in that step. This would then allow us to predict how the buffer evolves. This works because unlike achieved throughput, underlying capacity is an exogenous property of a network path and is not affected by the ABR actions.

However, underlying network capacity is a *latent* quantity — we do not observe it in our traces. The key challenge is therefore to *infer* such latent quantities from observational data. Concretely, in our running example, we wish to estimate the latent factors like network capacity in each step of a trace, using observations such as bitrate, chunk size, achieved throughput, etc.<sup>5</sup>

Inferring such *latent confounders* and using them for counterfactual prediction is the core issue in the field of causal inference [52, 53]. In this paper, we draw upon casual inference to develop CausalSim, a framework for unbiased trace-driven simulation that is particularly well-suited to networking. As discussed in §3 and §5, CausalSim exploits (1) the properties of latent factors in a simple, but effective, network model, and (2) certain distributional invariances present in training data collected via an RCT. By taking advantage of this structure in the data generation process, CausalSim can infer the latent factors underlying its input data and learn a causal model of network dynamics. As an illustration, Figure 1a shows the predicted buffer occupancy distribution when simulating FabABR on the traces of users assigned to BBA using CausalSim. As we can see, CausalSim matches the ground-truth distribution for FabABR much more accurately than the alternatives.

### 3 MODEL

#### 3.1 Causal Dynamics

We consider a discrete-time controlled dynamics system with partially observed state. Let  $t$  denote the time index, the state at time  $t$  be comprised of *observed state*  $o_t^*$  and *latent state*  $u_t$ , and  $a_t$  be the control or action chosen at time  $t$ . Then:

$$o_{t+1}^* = \mathcal{F}_{\text{evolution}}(o_t^*, u_t, a_t), \quad (1)$$

where  $\mathcal{F}_{\text{evolution}}$  models the system dynamics. We assume that the latent states are decided in an *exogenous* manner and are not impacted by the choice of actions. Such Structural Causal Models (SCM) with exogenous latent factors are widely used in the causal inference literature [52, 53].

The ABR example is an instance of such a model. Specifically, a time step corresponds to the download of a new chunk. The observable  $o_t^*$  represents playback buffer level, achieved

<sup>5</sup>For simplicity, we only mention network capacity here, but in reality there are other latent path conditions like the number of competing flows that could also affect achieved throughput, and the same reasoning applies to them.

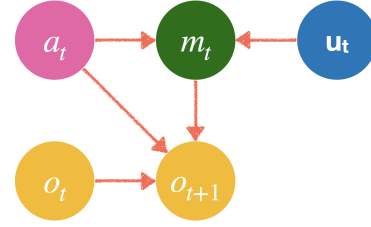


**Figure 2: Graphical version of discrete-time dynamical system equation with full mediation structure.**

throughput, Min RTT, and available chunk sizes, while  $u_t$  represents latent network conditions, e.g. bottleneck link speed, number of competing flows sharing the same path, type of congestion control used by competing flows, etc.

At each time step, a controller policy takes actions based on observation vector  $o_t^*$ . This action  $a_t$ , along with the state of the system  $(u_t, o_t^*)$  generates the next observation  $o_{t+1}^*$ .

Typically, latent network conditions are exogenous factors, beyond the impact of a particular user’s policy or actions. For instance, the bottleneck link speed, number of competing flows and type of congestion control that they use, are not affected by the actions of the ABR policy. On the other hand, a user’s actions directly impact what that user observes, e.g., the *achieved* throughput as discussed in §2.

As a further simplification, in some problems, the observable  $o_t^*$  includes a *mediator*<sup>6</sup>, which we refer to as  $m_t$ . It mediates the effect of latent network conditions on observations. In other words, we can divide  $o_t^*$  into two parts: mediator  $m_t$ , and the rest of observables  $o_t$ . Henceforth, the term “observation” will refer to  $o_t$  and not  $o_t^*$ . The mediator is sufficient to determine the *effect* of latent network conditions on the evolution of other observed quantities. Using this structure, we can substitute eq. (1) with the following two equations:

$$m_t = \mathcal{F}_{\text{mediation}}(a_t, u_t), \quad (2)$$

$$o_{t+1} = \mathcal{F}_{\text{system}}(o_t, m_t, a_t) \quad (3)$$

Figure 2 provides a visual depiction of this additional structure. The latest hidden network condition  $u_t$  and the action  $a_t$  generate the observed mediator  $m_t$ , which along with the previous observation  $o_t$  and the policy’s action  $a_t$ , determines the next observation  $o_{t+1}$ . It is worth emphasizing two differences between  $m_t$  and  $u_t$ : (i)  $m_t$  is observed, whereas  $u_t$  is latent; (ii)  $m_t$  is impacted by the actions, whereas  $u_t$  is exogenous.

In our running ABR example,  $m_t$  is the achieved throughput when downloading a chunk. Note that the achieved throughput depends on the ABR action as well as the latent network conditions. Equation (2) captures this relationship and is the source of the bias induced by the policy, which we described in §2.1.3 as the central issue for trace-driven simulation. Once the achieved throughput is revealed, it suffices to determine

<sup>6</sup>We borrow this term from the causal inference literature [52].

the evolution of other observed quantities like the playback buffer; no other information about the latent factors is needed.

### 3.2 Data

We are given  $N$  trajectories (network traces), collected using  $K$  specific policies. Let  $H_i$  be the length of trajectory  $i \in [N] \equiv \{1, \dots, N\}$ . For trajectory  $i \in [N]$ , we observe  $(m_t^i, o_t^i, a_t^i)_{t=1}^{H_i}$ . We assume that the traces are generated using an RCT, i.e. that each trace was assigned one of the  $K$  policies at random in the observed data.

### 3.3 Trace-Driven Simulation is Counterfactual Estimation

Our goal is to estimate the observations under an arbitrary given policy for each of the  $N$  trajectories. Let  $\{u_t^i\}_{t=1}^{H_i}$  be the exogenous latent network conditions for trajectory  $i \in [N]$ . Formally, for any given trajectory  $i \in [N]$  and given a sequence of actions  $\{\tilde{a}_t^i\}_{t=1}^{H_i}$ , starting with observation  $o_1^i$  and under the same sequence of latent network conditions  $\{u_t^i\}_{t=1}^{H_i}$ , we wish to estimate the counterfactual observations  $\{\tilde{o}_t^i\}_{t=1}^{H_i}$  that are consistent with eqs. (2) and (3).

This is counterfactual estimation since it requires (i) estimating latent  $\{u_t^i\}_{t=1}^{H_i}$  for observed trajectory  $i$  and using it along with the counterfactual actions  $\{\tilde{a}_t^i\}_{t=1}^{H_i}$  to predict counterfactual mediators  $\{\tilde{m}_t^i\}_{t=1}^{H_i}$  consistent with eq. (2), and then (ii) using counterfactual mediators and actions to predict counterfactual observations  $\{\tilde{o}_t^i\}_{t=1}^{H_i}$  consistent with eq. (3).

For (ii), learning  $\mathcal{F}_{\text{system}}$  is a supervised learning task because its inputs,  $(o_t, m_t, a_t)$ , and output,  $o_{t+1}$ , are fully observed. If  $\{u_t^i\}_{t=1}^{H_i}$  was observed, then (i) would also boil down to learning  $\mathcal{F}_{\text{mediation}}$  in a supervised manner. *It is the lack of observability of  $\{u_t^i\}_{t=1}^{H_i}$  that makes the task of simulation extremely challenging. In short, we are left with (i), the task of estimating  $\{\tilde{m}_t^i\}_{t=1}^{H_i}$  and learning  $\mathcal{F}_{\text{mediation}}$ .*

## 4 CAUSALSIM: KEY INSIGHTS

In this section, we discuss the key insights behind CausalSim. We show that counterfactual estimation can be viewed as a challenging variant of the matrix completion problem [6, 11], where very few entries of a matrix are observed (below information theoretic thresholds in the standard formulation) and these entries are not sampled at random (as is required by standard matrix completion procedures). We then discuss how a certain distributional invariance property that is present in data collected in an RCT allows us to complete the matrix.

### 4.1 Counterfactual Estimation as Matrix Completion

Recall the task of estimating the counterfactual mediators  $\{\tilde{m}_t^i\}_{t=1}^{H_i}$  consistent with eq. (2) (§3.3). In this section, we pose this task as a variant of the classical matrix completion problem. For simplicity, let action  $a_t$  be one of the finitely many options  $[A] = \{1, \dots, A\}$  for some  $A \geq 2$ . Imagine an  $A$  by  $U$  matrix  $M$ , where rows correspond to  $A$  potential actions, and columns corresponds to a  $U = \sum_{i=1}^N H_i$  latent network conditions ( $u_t^i$  for the different choices of  $i$  and  $t$ ) in the observed data. To order the columns, we may index  $u_t^i$  as a tuple  $(i, t)$  and order these tuples in lexicographic order. The matrix  $M$  is called the potential outcome matrix in the causal inference literature [56].

At the  $t$ -th step of the  $i$ -th trajectory, we observe  $m_t^i = \mathcal{F}_{\text{mediation}}(a_t^i, u_t^i)$ , which is the entry in  $M$  in the row corresponding to  $a_t^i$  and the column corresponding to  $u_t^i$ . The counterfactual quantities of interest,  $\tilde{m}_t^i = \mathcal{F}_{\text{mediation}}(\tilde{a}_t^i, u_t^i)$  for  $\tilde{a}_t^i \neq a_t^i$ , are the missing entries in  $M$  in the same column. In summary, we observe one entry per column of the matrix  $M$  and we wish to estimate the missing values in the matrix.

The question of completing or filling missing values in a matrix based on its partially observed entries is known as *Matrix completion* [15], a topic that has seen tremendous progress in the past two decades [14, 16, 43]. Matrix completion methods make some assumptions about the matrix and the revealed entries, which makes it possible to recover the whole matrix.

The first assumption these methods make is that the matrix has some structure such as being (approximately) low-rank. Low-rank structure holds in many real-world problems [64], and exploiting it has been fruitful in many domains (see §7 for details). Furthermore, prior work has observed low-rank structure in network measurements e.g. in traffic matrices [13, 38, 39, 55] and network distance (i.e. RTT) [42, 48, 61].

Low-rank structure roughly means that the data generation process is “simple” and can be explained by a small number of factors. We expect this to be true in many networking problems, because network path behaviors emerge from the interactions of a relatively small number of simple components (e.g., rate limiters, traffic policers, queue management schemes, link schedulers, congestion controllers, etc.). The emergent behavior can appear complex but the underlying components can typically be described (approximately) using simple functions. Although we have no way of knowing the true function  $\mathcal{F}_{\text{mediation}}$  underlying real-world data like the Puffer dataset, our successful counterfactual predictions (§6.1) suggest that the low rank structure exists. In §D.2, we use a simple model of congestion control to provide intuition on how low-rank structure can emerge in ABR data.

The second assumption of matrix completion methods is randomness in the pattern of missing entries. These methods



have a difficult time recovering the matrix if the missing pattern is not random, and depends on the latent factors, or the entries themselves [5]. In the ABR example, this assumption does not hold at all. Revealed entries are determined by the actions policies take based on some observations, and these observations often include the history of achieved throughput. This means that not only the missing pattern is not random, but it is a function of the matrix entries in previous columns.

The third assumption of matrix completion methods is that a large enough number of matrix entries are revealed. There exists an information-theoretic lower bound of  $4Ur - r^2$  on the minimum number of revealed elements for a matrix of rank  $r$  to be recoverable [35]. In our ABR example, only  $U$  matrix elements are revealed (one in each of  $U$  columns), which is at least 4 times less than the information-theoretic lower bound (assuming the low-rank structure i.e.  $r \ll U$ ). This means that the problem is highly under-specified [18].

In summary, the second and third assumptions do not hold in our ABR problem, so we cannot use *existing* matrix completion methods. However, as we shall argue, the existence of certain distributional invariance properties in the data implied by the RCT setting, makes matrix completion feasible.

To that end, consider an RCT setting where each of  $N$  trajectories is assigned to one of  $K$  policies completely at random. The key observation is that, if the latent exogenous network conditions across trajectories were generated from an (unknown) underlying distribution, then their distribution would remain the same for trajectories assigned to any of the  $K$  policies. In other words, since policies are assigned to paths at random, they all “experience” the same distribution of latent network conditions. The fact that distribution of latent network conditions is policy invariant helps recover the matrix, as we show next through a simple example.

## 4.2 Exploiting the Policy Invariance of Latent Factors

Consider a very simple example where  $A = 2$  and  $U = 2n$ , and the rank of potential outcome matrix  $M$  is equal to 1. Rank 1 means  $M = au^T$  for some  $a \in \mathbb{R}^2$  and  $u \in \mathbb{R}^{2n}$  with  $M_{i,j} = a_i \cdot u_j$  for  $i \in [2], j \in [2n]$ .<sup>7</sup> Suppose we have  $K = 2$  simple policies, where each policy always chooses only one of the two actions. Furthermore, we consider an RCT setting. That is, the distribution of latent network conditions across trajectories assigned to both policies should be the same.

Without loss of generality, we can re-order the columns of  $M$  so that the first  $n$  columns correspond to the latent exogenous states of the trajectories assigned to policy 1, and the second  $n$  columns are those assigned to policy 2. Then

<sup>7</sup>Note that for readability, we are slightly abusing notation in this example by using  $a$  and  $u$  for the factorization and thereby, overloading them.

the observed entries of matrix  $M$  appear as

$$\begin{bmatrix} M_{1,1} & M_{1,2} & \dots & M_{1,n} & \star & \dots & \star & \star \\ \star & \star & \dots & \star & M_{2,n+1} & \dots & M_{2,2n-1} & M_{1,2n}, \end{bmatrix}$$

where  $\star$  represents the missing values.

Let’s consider recovering the missing observation  $M_{2,1}$ . For column 1, we know the observation under the first action, i.e.  $M_{1,1}$ . Due to rank 1 structure, we have

$$\frac{M_{2,1}}{M_{1,1}} = \frac{a_2 u_1}{a_1 u_1} = \frac{a_2}{a_1}. \quad (4)$$

Therefore, to find  $M_{2,1}$  (and by a similar argument, to find all missing entries of  $M$ ), we need to estimate the ratio  $\frac{a_2}{a_1}$ .

Due to the distributional invariance induced by RCT, the samples  $u_1, \dots, u_n$  (which correspond to the latent factors encountered by policy 1) come from the same distribution as the samples  $u_{n+1}, \dots, u_{2n}$  (which correspond to the latent factors encountered by policy 2), for large enough  $n$ . Thus, their expected value should be equal. Precisely,

$$\frac{1}{n} \sum_{j=1}^n u_j \approx \frac{1}{n} \sum_{j=n+1}^{2n} u_j. \quad (5)$$

However, we do not have access to the latent  $u$ ! But (5) implies

$$\frac{\sum_{j=1}^n M_{1,j}}{\sum_{j=n+1}^{2n} M_{2,j}} = \frac{\sum_{j=1}^n a_1 \cdot u_j}{\sum_{j=n+1}^{2n} a_2 \cdot u_j} \approx \frac{a_1}{a_2}. \quad (6)$$

This provides precisely the quantity of interest in (4) based on the observed entries, enabling us to complete the matrix.

This simple illustrative example relied on a convenient observational pattern (based on policies that always choose one action) and rank 1 structure. But the idea can be generalized. For a generic setting with rank  $r$ , and the observational pattern required to complete the matrix in the general setting, refer to Appendix A. Roughly, it shows that we can still recover the matrix if entries of  $M$  are  $m$ -dimensional and  $m \geq r$  where  $r$  is the rank, and also policies used in the RCT have the following three conditions: 1)  $K \geq r \times A$ , 2) policies are sufficiently diverse, and 3) have good coverage of the action space.

## 5 CAUSALSIM: DETAILS

The analytical method described in §4.2 (and its generalization in Appendix A) is usually not applicable in practice, since it relies on strict assumptions. For example, the matrix  $M$  must be exactly rank  $r$ ; if it is approximately rank  $r$ , we have found the calculation can be brittle. Moreover, the method above only uses invariance of the mean of the latent factors. However, we know that the invariance property holds for distribution of the latent factors in an RCT, and not only the mean. Potentially, using invariance of higher moments as well could help relax its assumptions.

This section describes the details of CausalSim, a practical method that overcomes these drawbacks. CausalSim builds

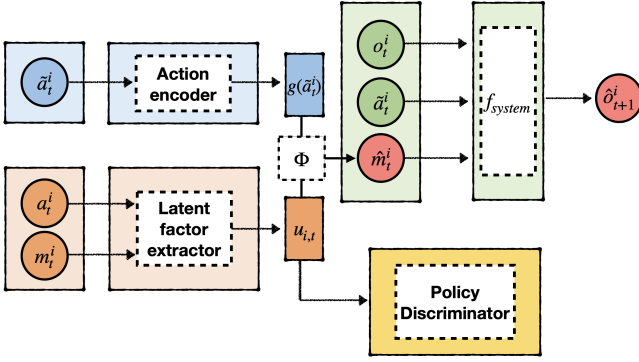


**Figure 3: Algorithmic architecture of CausalSim. Dashed boxes indicate neural networks.**

upon the insights presented earlier but replaces the analytical calculation with a learning algorithm.

**Algorithmic architecture.** As discussed, using observed data, CausalSim aims to learn  $u_t^i : t \leq H_i, i \leq N$ ,  $\mathcal{F}_{\text{mediation}}$  and  $\mathcal{F}_{\text{system}}$ . Figure 3 summarizes the algorithmic architecture of CausalSim to learn them.

From the lens of matrix completion as discussed earlier,  $m_t^i \approx g(a_t^i)^T u_t^i$ , (i.e. “dot product” between vectors  $g(a_t^i)$  and  $u_t^i$ ), where  $g(a_t^i)$  is an encoding of action  $a_t^i$ . For a potential outcome matrix  $M$  of (approximate) rank  $r$ , both  $u_t^i$  and  $g(a_t^i)$  can be assumed to belong to  $\mathbb{R}^r$ . More generally, matrix completion suggests a *factorized* structure where  $m_t^i \approx \Phi(g(a_t^i), u_t^i)$ , i.e.  $m_t^i$  is a generic function applied to  $g(a_t^i)$  and  $u_t^i$ . Replacing a traditional “dot product” with a generic function  $\Phi$  (e.g. a Multi Layer Perceptron (MLP)) provides model flexibility, which we exercise in our experiments.

CausalSim uses observed trajectories  $(o_{t+1}^i, o_t^i, m_t^i, a_t^i) : t < H_i, i \leq N$  to learn the *action encoder*  $g$ , the *latent factor extractor* which extracts  $u_t^i$  from  $a_t^i$  and  $m_t^i$ , the *generalized dot product*  $\Phi$ , and a mapping  $\mathcal{F}_{\text{system}}$ , all using MLPs.

**Loss function.** The loss function imposes consistency with observed data, and invariance induced by the RCT.

In particular, we use quadratic loss between the estimated  $\hat{m}_t^i$  and observed  $m_t^i$  and also quadratic loss between  $\hat{o}_t^i$  and observed  $o_t^i$  to enforce consistency with the observations.

For the distributional invariance (due to RCT) across the learned  $u_t^i : t \leq H_i, i \leq N$  we need to make sure that the distribution of latent factors  $u$  across policies is identical. To that end, we utilize a *discriminator* neural network. Such neural networks have been considered in the paradigm of adversarial learning [24, 63]. Specifically, the policy discriminator aims to predict the policy  $\pi \in [K]$  that took action  $a_t^i$  from the learned latent state  $u_t^i$  (see Figure 3). Towards that, we use a cross-entropy loss to train the policy discriminator:

$$\mathcal{L}_{\text{disc}} = \mathbb{E}_D[-\log(\mathbb{P}(\pi|\hat{u}))], \quad (7)$$

where the expectation is over the training dataset  $D$ .

If the extracted latent factors are policy invariant, the policy discriminator should do no better at this task than guessing at random. Hence our goal is to ensure that the policy discriminator’s predictions are as uniform as possible across all policies, and we use this as a training signal for other components.

**Training procedure.** CausalSim’s training procedure alternates between: (i) training the policy discriminator using the loss  $\mathcal{L}_{\text{disc}}$  and the ground truth policy labels; and (ii) fixing the discriminator and training other components using an aggregated loss  $\mathcal{L}_{\text{total}}$ . This aggregated loss, in its most general form, combines the negated discriminator loss with the two aforementioned quadratic losses using a mixing hyper-parameter  $\kappa$ .

$$\mathcal{L}_{\text{total}} = \mathbb{E}_D \left[ \delta(m_t^i - \hat{m}_t^i)^2 + (o_t^i - \hat{o}_t^i)^2 \right] - \kappa \mathcal{L}_{\text{disc}}. \quad (8)$$

Note the negative sign of discriminator loss, which means we train other components to maximize discriminator loss i.e. fool the discriminator to ensure policy invariance as described above. Algorithm 1 in the appendix provides a detailed description of CausalSim’s training procedure.

**Counterfactual estimation.** To produce counterfactual estimates, as described above, the  $u_t^i : t \leq H_i, i \leq N$  are extracted from observed data. Counterfactual actions  $\tilde{a}_t^i$  are encoded with learned mapping  $g(\cdot)$  and the counterfactual mediators  $\tilde{m}_t^i$  are estimated through factorization (i.e. the function  $\Phi$ ). Using the inferred counterfactual mediators, along with the learned system function  $\mathcal{F}_{\text{system}}$ , we start with  $o_1^i$  and predict counterfactual observations  $\hat{o}_t^i : t \leq H_i, i \leq N$ , one step at a time.

## 6 EVALUATION

We evaluate CausalSim using one real-world and two synthetic datasets, comparing its performance with two baselines:

- *ExpertSim* from §2.1.1: Uses a system expert’s knowledge for simulation.
- *SLSim* from §2.1.2: Uses a standard supervised-learning technique to learn dynamics of the system from data.

We evaluate CausalSim’s ability to do accurate counterfactual simulation (§6.1 and §6.3) and its application in policy learning and optimization using offline trace data (§6.2).

### 6.1 A Real-world ABR Experiment

Our real-world ABR dataset comes from Puffer [65], a research project that evaluates ABR algorithms in an RCT setting with real video streaming sessions. Whenever a client initiates a video streaming session in Puffer’s website, a random ABR algorithm is chosen and assigned to that session. Sessions are logged (buffer levels, chunk sizes, timestamps, download times, etc) anonymously and the data is available for public use. We use the trajectories in these logs as data for training and evaluation. Each of these trajectories uses



one of the five ABR algorithms (linear BBA, BOLA-BASIC v1, BOLA-BASIC v2, Fugu-CL, Fugu-2019), assigned at random. Further details of the setup can be found in §C.5.

**6.1.1 Can CausalSim Simulate a New Policy?** We choose one of BBA, BOLA-BASIC v1, and BOLA-BASIC v2<sup>8</sup> as the new policy that we want to simulate, and call it the *target* policy. The remaining four policies are called *source* policies. Trajectories assigned to the four source policies comprise our training dataset, which we use for training CausalSim and the two baselines. The goal is to simulate the outcome of applying the target policy on trajectories assigned to one of the source policies.

Ideally, we need ground-truth labels to evaluate the simulation performance. However, we do not have access to these labels because each trace is only assigned to a single policy in the Puffer dataset. To overcome this issue, we resort to distributional evaluation. Puffer data is collected in an RCT setting, which means that the characteristics of network paths assigned to each policy is the same. Therefore, if we accurately simulate the target policy on trajectories assigned to one of the source policies, the distribution of each variable (e.g. buffer level) must be similar in simulated trajectories and actual trajectories assigned to the target policy. This motivates using similarity of the two distributions as our performance metric.

To quantify the similarity of two distributions, we use the Earth Mover Distance (EMD) [57]. We can calculate EMD for one-dimensional distributions as:

$$\text{EMD}(\mathcal{P}, \mathcal{Q}) = \int_{-\infty}^{+\infty} |\mathcal{P}(x) - \mathcal{Q}(x)| dx,$$

where  $\mathcal{P}$  and  $\mathcal{Q}$  are the Cumulative Distribution Function (CDF) of  $p$  and  $q$ , respectively. A small EMD between two distributions implies that they are similar.

Figure 4a shows the CDF of the EMD (between actual and simulated buffer level distributions) for CausalSim and baselines, over all possible source/target policy pairs. EMD of CausalSim is smaller than EMD of baselines across almost all experiments. In terms of the median EMD across all experiments, CausalSim bests ExpertSim and SLSim by 44% and 53% respectively. Figure 1a shows the source, target, and simulated buffer level distribution in a typical scenario, where BBA and BOLA-BASIC-v1 are source and target policies respectively.

In about 30% of cases, SLSim is slightly better than CausalSim. These cases are “easy” simulation scenarios where the source and target policies make similar actions (For more details see §C.2). In these cases, the EMD is low for both CausalSim and baseline simulators ( $< 0.2$ ), and all perform well. For instance, Figure 8i (in the Appendix) shows source, target, and simulated buffer level distribution in an easy scenario, where

<sup>8</sup>We exclude Fugu as a test policy since it requires access to some TCP information which is not logged in the dataset (see §C.5).

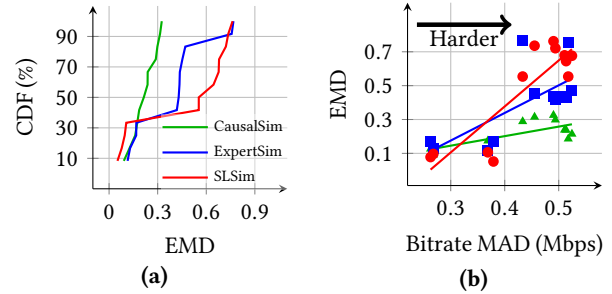


**Figure 4: On average, CausalSim bests ExpertSim and SLSim by 44% and 53% respectively, based on the EMD distance metric. Left: Distribution of CausalSim, ExpertSim, and SLSim EMDs over all possible source/target choices. Right: Error (EMD) increases for baseline as simulation scenarios get harder, but CausalSim maintains good accuracy.**

BOLA-BASIC-v2 and Fugu-2019 are the target and source policies respectively. In this example, all simulated distributions match the target distribution quite well. We provide plots for all combinations of source and target policies in Figure 8.

Figure 4b shows where CausalSim most shines i.e. hard simulation scenarios. The Y-axis is the error (EMD), and the X-axis is the mean absolute difference (MAD) between actions taken by the source policy and the target policy, in SLSim simulation. The larger the action difference, the harder the scenario (§C.2). As we move toward harder scenarios, error increase for baselines. However, CausalSim is robust to the difficulty of simulation.

**6.1.2 Additional experiments.** We perform further evaluations of CausalSim in the ABR environment. Due to space constraints, we summarize these results here and defer details to the appendix.

**A more fine-grained evaluation.** In the results above, we evaluate the performance of CausalSim and baselines using the distribution of buffer occupancy across the whole population. One way to further validate the results is to test whether they will hold on carefully partitioned sub-populations. In §C.3, we show that this is indeed the case when the sub-populations are partitioned according to the Min Round Trip Time (RTT), a network property that is independent of the selected ABR algorithm in Puffer.

**Hyperparameters tuning.** Counterfactual estimation (§3.3) is inherently an Out of Distribution (OOD) prediction task. Hence, typical supervised-learning hyper-parameter tuning methods do not work. In §C.4, we describe and evaluate CausalSim’s hyper-parameter tuning procedure.

**Ground truth evaluation.** Real data never comes with ground truth counterfactual labels. As a result, we cannot evaluate CausalSim’s simulations for each time step in real data, but we can do this in a synthetic environment. In §D.3,

we evaluate CausalSim using ground truth counterfactual labels and show that it still outperforms baselines. Specifically, CausalSim achieves a MAPE of ( $\sim 5\%$ ), which is significantly lower than both ExpertSim’s and SLSim’s ( $\sim 10\%$ ).

## 6.2 Learning ABR policies with CausalSim

We observed how CausalSim can simulate a real-world ABR environment more accurately compared to baselines, and therefore better evaluate newly proposed algorithms. We now take these experiments one step further and ask *can CausalSim be used to design better policies using offline trace data?*

Recent work has shown that reinforcement learning (RL) algorithms can learn strong ABR policies by learning through interactions with the environment [46]. Could we use a CausalSim model to train high-performance ABR policies without direct environment interaction? Ideally, we would investigate this by training RL policies with each simulator trained on the Puffer dataset, and would evaluate the policies on the running Puffer framework. The authors of Puffer point out, however, that it took 8 months of continual data collection to be able to dial down the statistical variance in the results and make statistically significant comparisons between ABR policies. As such, we decided to carry out an initial experiment in the aforementioned synthetic ABR environment. This allows us to rapidly evaluate policies across a large number of network traces, and importantly, to compare policies on the same set of traces eliminating an important source of variability. Our synthetic environment uses a basic model of congestion control it to capture the relationship between chunk size and achieved throughput for paths with different capacity and RTT, and it uses a statistical model to generate a wide variety of network capacity behavior (e.g., different average bandwidth, variability, etc.). We build a CausalSim model using traces from a “simulated RCT” on the synthetic environment. For a full explanation of the simulation setup, network capacity generation procedure, and the simulated policies, refer to §D.4 in the appendix.

**Performance Metric.** ABR algorithms are typically evaluated through QoE metrics [67]. Assuming the chosen bitrate at step  $t$  was  $q_t$ , the download time was  $d_t$  and the buffer was  $b_t$ , we use the following QoE definition:

$$QoE_t = q_t - |q_t - q_{t-1}| - \mu \cdot \max(0, d_t - b_{t-1})$$

This QoE metric captures three goals (in succession): 1) Stream in high quality, 2) Maintain a stable quality, 3) Avoid rebuffering. Better policies yield higher QoE values, where an ideal QoE is equal to the max bitrate.

**6.2.1 How to train policies via simulators?** To train the RL agent, we take a set of logged trajectories where the source policy was MPC and feed them to CausalSim. In each step, CausalSim will predict the next counterfactual observation and reward, and the RL agent will choose the next counterfactual action based on that observation. This

process repeats until this simulated session is over, after which the counterfactual trajectory is used to train the RL agent. For the RL algorithm, we utilize the Advantage Actor Critic (A2C) method, a prominent on-policy algorithm, along with Generalized Advantage Estimation (GAE). For a detailed description of the setup and hyperparameters refer to §D.6.

**6.2.2 Does CausalSim train better policies?** Figure 5a plots the CDF of average session QoE that each policy attains. Here, *Real Environment* refers to training directly with the synthetic ABR environment, and CausalSim, ExpertSim and SLSim refer to policies trained by using each of these simulators. CausalSim trains policies nearly as well as training directly on the environment, while ExpertSim and SLSim fail to provide robust policies across all sessions. Figure 5b plots the CDFs for the high RTT (above 300 ms) clients, where the gap between CausalSim and the baseline simulators is even larger.

In this environment, chunk are downloaded according to a slow start model, where congestion control must ramp up its window size over several RTTs before the download rate can reach the available bandwidth. As a result, downloads of smaller chunks (with lower bitrates) incur a noticeable overhead, particularly on high-RTT paths. This overhead becomes less apparent as chosen bitrates become larger. Biased simulators such as SLSim and ExpertSim, which assume all actions lead to the same observed bandwidth, overestimate the achieved rate when counterfactual bitrates are smaller than factual ones (chosen by the source policy) and underestimate it when the counterfactual bitrates are larger. Since the source policy is conservative and tends to choose low bitrates, ExpertSim and SLSim find larger bitrates to be undesirable in the QoE trade-off. This can be seen in Figure 5c, which visualizes the 3 aspects of QoE in terms of rebuffering rate and the smoothed bitrate, i.e the chosen bitrates with the smoothness penalty. Notice how policies trained on the real environment and CausalSim utilize the network by 200 kbps more than other policies. The extra rebuffering that CausalSim incurs is negligible compared to the extra bitrate: 5.9 seconds every hour.

## 6.3 Server Load Balancing

We now apply CausalSim to a second use case, server load balancing, to evaluate its versatility.

**6.3.1 Environment Setup and Simulation Dynamics.** We consider a Load Balancing problem with heterogeneous servers. This synthetic environment consists of  $N = 8$  servers (and a queue for each) with different processing powers, a load balancer, and a series of jobs that need to be processed on these servers. Each job has a specific size which is unknown to the load balancer. Each server can process jobs at a specific rate  $\{r_i\}_{i=1}^N$ , which is also unknown to the load balancer. The load balancer receives jobs and must assign them to one of  $N$  servers. Assuming the  $k^{\text{th}}$  arriving job has size  $S_k$  and gets assigned to server  $a_k$ , the job processing time will be  $S_k/r_{a_k}$ .

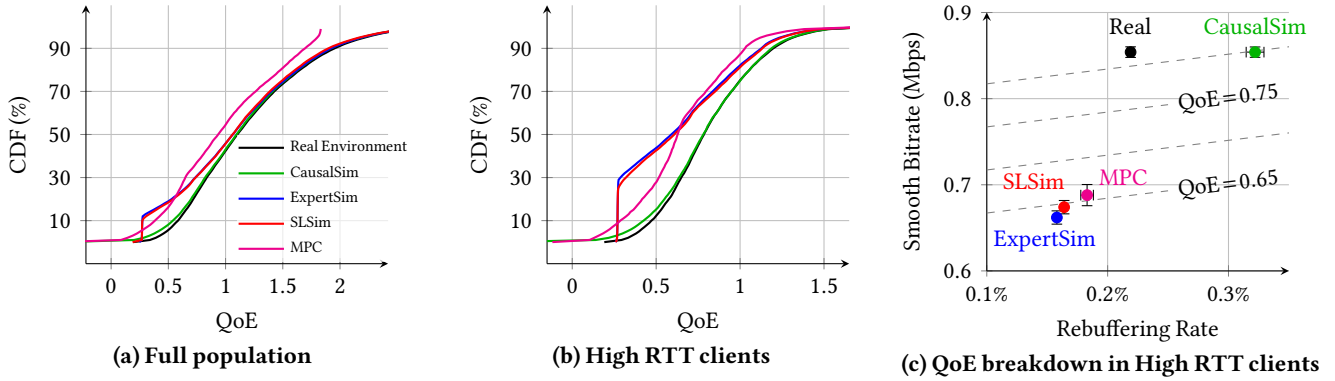


**Figure 5: CausalSim trained policies perform well, only marginally behind training on the real environment. Distribution of Quality of Experience (QoE) in policies trained with the real environment, CausalSim, ExpertSim, and the MPC policy. CausalSim does not underestimate bandwidth in high RTT clients and trains policies that strike the best balance in QoE goals.**

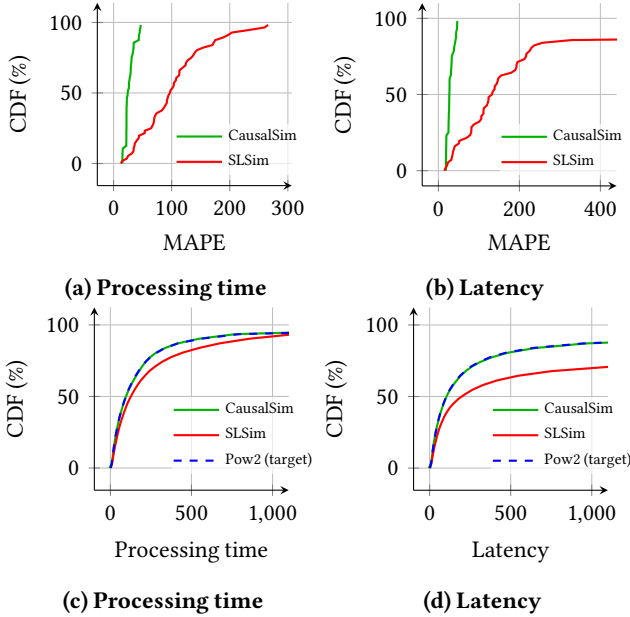


**Figure 6: Top: Distribution of CausalSim, and SLSim MAPEs over all source target pairs. Bottom: Distribution of CausalSim, and SLSim predictions under Power of Two policy and how it compares to the actual distribution.**

If this job is not blocked by some other job being processed, its latency will equal its processing time. If it is blocked, and the jobs ahead of it in the queue take  $T_k$  to be processed, the incurred latency is  $S_k/r_{a_k} + T_k$ .

In our simulation, we generate a collection of 5000 trajectories each with 1000 steps and use 16 policies in the load balancer. For a detailed explanation of the policies, job size generation process, and server processing rates, refer to §E.1.

**6.3.2 Experiment setup.** The aim of this experiment is to evaluate whether we can simulate new unseen test policies in this environment, given observations of processing time

from other training policies. Note that while we observe the processing time of each job, the actual size of the job is not observed, i.e., it is the latent state in this problem. For both CausalSim and the baseline, we assume access to  $\mathcal{F}_{\text{system}}$  and focus on the more challenging task of estimating the mediator quantities  $m_i^t$  for  $i \leq 5000$ , and  $t \leq 1000$ . In load balancing, the mediator quantity which mediates the effect of the latent state (job size) on the observations (latency) is the processing time. In other words, the counterfactual task is to estimate the processing time of a job on servers other than the one that it actually ran on (without knowing either the job size or the server processing rates).

In the absence of an expert baseline analogous to that of the ABR experiments, we compare CausalSim against SLSim. Specifically, in this adapted variant of SLSim, the input to the neural network is the observed processing time and the target server, and its output is the processing time under the targeted server. Despite its simplicity, this setup presents an interesting challenge for SLSim. While training the observed and target processing time are always the same, and hence it is almost impossible for SLSim to learn the true dynamics (e.g., the server’s underlying processing power). As we show next, CausalSim sidesteps this problem by estimating policy invariant latent states. For details regarding the network architecture and training details for both SLSim and CausalSim, refer to Table 7 in the appendix.

**Performance Metric.** We compare CausalSim and SLSim predictions with the underlying ground truth through the Mean Absolute Percentage Error (MAPE) metric. Let  $\hat{\mathbf{p}} = \{\hat{p}_i\}_{i=1}^N$  and  $\mathbf{p} = \{p_i\}_{i=1}^N$  denotes the vectors of predicted and ground truth quantity of interest, respectively. Then, MAPE is defined as:

$$\text{MAPE}(\mathbf{p}, \hat{\mathbf{p}}) = \frac{100}{N} \sum_{i=1}^N \frac{|\hat{p}_i - p_i|}{p_i}.$$

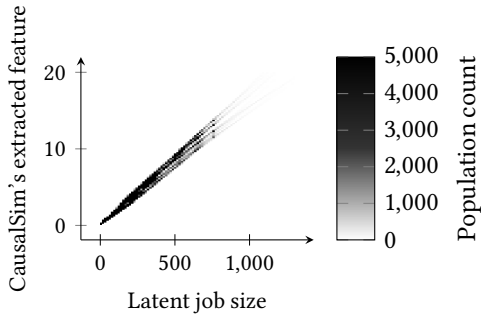


**Figure 7: Two-dimensional histogram heatmap of CausalSim extracted latent state vs. latent job sizes.**

**6.3.3 Can CausalSim Faithfully Simulate New Policies?** As is done in the ABR case studies, we train CausalSim and SLSim models based on a dataset generated using all policies except one, which will be the target policy. We use the same hyperparameter tuning approach explained in §C.4. We carry out this evaluation on eight target policies. We evaluate the performance for each pair of source-target policies, as was done in §6.1. In total, we have 120 different source/target policy pairs.

In Figure 6a and Figure 6b, we show the CDF of the MAPE of estimating the processing time and the latency, respectively, using both CausalSim and SLSim. As evident in these two figures, CausalSim’s error is significantly lower than that of SLSim for both the processing time and latency. In particular, the average MAPE when estimating processing time/latency is 27.1%/29.1% for CausalSim and 102.4%/240.8% for SLSim.

Further evidence of the accuracy of CausalSim counterfactual predictions is illustrated in Figure 6c and Figure 6d. Specifically, the two figures show the distribution of the actual and estimated (using CausalSim and SLSim) processing time and latency under the *Power of Two* policy using the random policy as the source policy. The two figures show how well CausalSim estimates the performance of a target policy, as its estimates distribution is virtually identical to the actual distribution. In contrast, SLSim overestimates these quantities.

**6.3.4 Does CausalSim Faithfully Infer Latent States?** We test the claim that estimating the exogenous latent state and using it to predict the next state was indeed the key to producing accurate counterfactual predictions, as the architecture of CausalSim suggests. To do so, we compare CausalSim’s estimated latent state with the underlying job sizes—the job size is indeed the latent state that dictates the dynamics in the load balancing environment. We find that the estimated latent states and the job sizes are highly correlated, as illustrated in Figure 7, with a PCC of 0.994. This demonstrates that CausalSim can learn faithful representations of true latent states.

## 7 RELATED-WORK

**Data-driven simulation and policy evaluation in systems and networking.** Packet level simulators [17, 26, 40]

tend to sacrifice either scalability or accuracy when simulating large networks. Recent research combines machine learning with packet-level modeling to improve speed and accuracy of datacenter [69] and wide-area network [10] simulators. For instance, MimicNet [69] uses full fidelity simulation of a small portion of a datacenter to learn a mimic model, and replaces other portions of datacenter with the mimic to improve simulation speed. However, it avoids bias by requiring the full fidelity simulation in the training step to have the same configuration (e.g. congestion control protocol and workload) as the whole datacenter simulation step. There has been a surge in the use of data-driven optimization in network systems [45–47] to propose superior control algorithms. These works often evaluate their proposals on a set of traces, but trace-driven evaluation can be problematic [12, 65] because of the skews in the traces caused by the logging strategy and also the lack of coverage for certain sub-populations. Re-weighting schemes such as like Inverse Propensity Scoring [28] aim to mitigate the aforementioned skew, by accounting for the difference between the logging and the evaluation policy [32, 41]. Re-weighting schemes suffer from variance, especially in long trajectories, if the logging and evaluation policies are not similar. Furthermore, these schemes typically rely on random data collection policies, which are unrealistic to run in many production network settings. Doubly Robust techniques [12] aim to reduce both variance and bias by combining model-based and re-weighting based methods. Generally, such policy evaluation methods cannot respond to counterfactual questions at sub population or personalized levels, such as a single trajectory. What-If Scenario Evaluator (WISE) [62] builds a Causal Bayesian Network from the data that is able to answer what-if (intervention) questions. However, their method requires no latent confounding variables in the problem setting.

Unlike policy evaluation methods, CausalSim can do counterfactual estimation, with which one can do policy evaluation as well. Recent work [59] assumes a known latent bandwidth process in a synthetic environment to motivate counterfactual estimation for ABR simulation and identify latent bandwidth as a confounder, but fails to come up with a general solution. **Causal Inference.** Identifying causal relationships from observational data is a critical problem in many domains [25], including medicine [50], epidemiology [54], economics [31], and education [20]. Indeed, identifying causal structure and answering causal inference queries is an emerging theme in different machine learning tasks recently, including computer vision [66, 68], reinforcement learning [3, 22], fairness [23], and time-series analysis [4] to name a few. One important aspect about causal inference is its ability to answer counterfactual queries. For such queries, many methods were developed; where some approaches are motivated by Pearl’s structural causal model [52], and by Rubin’s potential

outcome framework [56]. We refer the interested reader to recent surveys such as [25] and references there in for an overview of recent advances in our ability to infer causal relationships from observational data.

Another related line of work within this literature is synthetic controls and its extension synthetic interventions, which aims to build synthetic trajectories of different units (e.g. individuals, geographic locations) under unseen interventions by appropriately learning across observed trajectories [1, 2, 6–9]. However, these approaches assume a static set of intervention and do not apply to our setting.

## 8 CONCLUDING REMARKS

CausalSim provides a simple and general solution for unbiased trace-driven simulation of network protocols, as we showcase in this paper using both synthetic and real-world data. The success of this approach has many implications. One major implication is that RCT data can be harnessed to provide a more robust and accessible benchmark for researchers to evaluate new algorithms. Further, our evaluations with synthetic data show that CausalSim provides accurate point-wise counterfactual predictions; this suggests that one may be able to use CausalSim to design and evaluate personalized policies for specific scenarios/users.

CausalSim is successful in problems with low-dimensional states. Evaluating it in problems with a higher-dimensional latent factors is an avenue for empirical work.

Moreover, in §4.2 and further in §A, we took an important step in identifying requirements for CausalSim to work, i.e. observation dimensionality and policy requirements. However, the theoretical method and its analysis was only exploiting the invariance of the mean of the latent factors, while the invariance property holds for the distribution of latent factors in an RCT. We believe that exploiting invariance of higher moments can relax the current assumptions needed in our analysis, which we leave as an interesting theoretical future work.

## 9 ACKNOWLEDGEMENT

We thank the Puffer team, and specifically Emily Marx for providing us with the data we used in §6.1.

## REFERENCES

- [1] A. Abadie, A. Diamond, and J. Hainmueller. 2010. Synthetic Control Methods for Comparative Case Studies: Estimating the Effect of California’s Tobacco Control Program. *J. Amer. Statist. Assoc.* (2010).
- [2] A. Abadie and J. Gardeazabal. 2003. The Economic Costs of Conflict: A Case Study of the Basque Country. *American Economic Review* (2003).
- [3] Anish Agarwal, Abdullah Alomar, Varkey Alumootil, Devavrat Shah, Dennis Shen, Zhi Xu, and Cindy Yang. 2021. PerSim: Data-Efficient Offline Reinforcement Learning with Heterogeneous Agents via Personalized Simulators. *arXiv preprint arXiv:2102.06961* (2021).
- [4] Anish Agarwal, Abdullah Alomar, and Devavrat Shah. 2020. On Multivariate Singular Spectrum Analysis. *arXiv e-prints* (2020), arXiv–2006.
- [5] Anish Agarwal, Munther A. Dahleh, Devavrat Shah, and Dennis Shen. 2021. Causal Matrix Completion. *ArXiv abs/2109.15154* (2021).
- [6] Anish Agarwal, Devavrat Shah, and Dennis Shen. 2021. Synthetic interventions. *arXiv preprint arXiv:2006.07691* (2021).
- [7] Anish Agarwal, Devavrat Shah, Dennis Shen, and Dogyoon Song. 2021. On robustness of principal component regression. *J. Amer. Statist. Assoc.* (2021).
- [8] Muhammad Amjad, Vishal Misra, Devavrat Shah, and Dennis Shen. 2019. MRSC: Multi-Dimensional Robust Synthetic Control. *Proc. ACM Meas. Anal. Comput. Syst.* 3, 2, Article 37 (June 2019), 27 pages. <https://doi.org/10.1145/3341617.3326152>
- [9] Muhammad Amjad, Devavrat Shah, and Dennis Shen. 2018. Robust Synthetic Control. *Journal of Machine Learning Research* 19, 22 (2018), 1–51. <http://jmlr.org/papers/v19/17-777.html>
- [10] Sachin Ashok, Sai Surya Duvvuri, Nagarajan Natarajan, Venkata N Padmanabhan, Sundararajan Sellamanickam, and Johannes Gehrke. 2020. iBox: Internet in a Box. In *Proceedings of the 19th ACM Workshop on Hot Topics in Networks*. 23–29.
- [11] Susan Athey, Mohsen Bayati, Nikolay Doudchenko, Guido Imbens, and Khashayar Khosravi. 2021. Matrix completion methods for causal panel data models. *J. Amer. Statist. Assoc.* (2021), 1–15.
- [12] Mihovil Bartulovic, Junchen Jiang, Sivaraman Balakrishnan, Vyas Sekar, and Bruno Sinopoli. 2017. Biases in data-driven networking, and what to do about them. In *Proceedings of the 16th ACM Workshop on Hot Topics in Networks*. 192–198.
- [13] Vineet Bharti, Pankaj Kankar, Lokesh Setia, Gonca Gürsun, Anukool Lakhina, and Mark Crovella. 2010. Inferring Invisible Traffic. In *Proceedings of the 6th International Conference (Co-NEXT ’10)*. Association for Computing Machinery, New York, NY, USA, Article 22, 12 pages. <https://doi.org/10.1145/1921168.1921197>
- [14] Changxiao Cai, Gen Li, Yuejie Chi, H Vincent Poor, and Yuxin Chen. 2021. Subspace estimation from unbalanced and incomplete data matrices:  $\ell_{2,\infty}$  statistical guarantees. *The Annals of Statistics* 49, 2 (2021), 944–967.
- [15] Emmanuel J Candès and Benjamin Recht. 2009. Exact matrix completion via convex optimization. *Foundations of Computational mathematics* 9, 6 (2009), 717–772.
- [16] Emmanuel J Candès and Terence Tao. 2010. The power of convex relaxation: Near-optimal matrix completion. *IEEE Transactions on Information Theory* 56, 5 (2010), 2053–2080.
- [17] Xinjie Chang. 1999. Network Simulations with OPNET. In *Proceedings of the 31st Conference on Winter Simulation: Simulation—a Bridge to the Future - Volume 1 (WSC ’99)*. Association for Computing Machinery, New York, NY, USA, 307–314. <https://doi.org/10.1145/324138.324232>
- [18] Alexander D’Amour, Katherine Heller, Dan Moldovan, Ben Adlam, Babak Alipanahi, Alex Beutel, Christina Chen, Jonathan Deaton, Jacob Eisenstein, Matthew D Hoffman, et al. 2020. Underspecification presents challenges for credibility in modern machine learning. *arXiv preprint arXiv:2011.03395* (2020).
- [19] DASH Industry Form. 2016. Reference Client 2.4.0. (2016). <http://mediapm.edgesuite.net/dash/public/nightly/samples/dash-if-reference-player/index.html>
- [20] Rajeev H Dehejia and Sadek Wahba. 1999. Causal effects in nonexperimental studies: Reevaluating the evaluation of training programs. *Journal of the American statistical Association* 94, 448 (1999), 1053–1062.
- [21] Sally Floyd and Vern Paxson. 2001. Difficulties in simulating the Internet. *IEEE/ACM Transactions on Networking* 9, 4 (2001), 392–403.
- [22] Andrew Forney, Judea Pearl, and Elias Bareinboim. 2017. Counterfactual data-fusion for online reinforcement learners. In *International Conference on Machine Learning*. PMLR, 1156–1164.
- [23] Sahaj Garg, Vincent Perot, Nicole Limtiaco, Ankur Taly, Ed H Chi, and Alex Beutel. 2019. Counterfactual fairness in text classification through robustness. In *Proceedings of the 2019 AAAI/ACM Conference on AI*,

- Ethics, and Society*. 219–226.
- [24] Ian Goodfellow, Jean Pouget-Abadie, Mehdi Mirza, Bing Xu, David Warde-Farley, Sherjil Ozair, Aaron Courville, and Yoshua Bengio. 2020. Generative adversarial networks. *Commun. ACM* 63, 11 (2020), 139–144.
- [25] Ruocheng Guo, Lu Cheng, Jundong Li, P Richard Hahn, and Huan Liu. 2020. A survey of learning causality with data: Problems and methods. *ACM Computing Surveys (CSUR)* 53, 4 (2020), 1–37.
- [26] Thomas R Henderson, Mathieu Lacage, George F Riley, Craig Dowell, and Joseph Kopena. 2008. Network simulations with the ns-3 simulator. *SIGCOMM demonstration* 14, 14 (2008), 527.
- [27] Paul W Holland. 1986. Statistics and causal inference. *Journal of the American statistical Association* 81, 396 (1986), 945–960.
- [28] Daniel G Horvitz and Donovan J Thompson. 1952. A generalization of sampling without replacement from a finite universe. *Journal of the American statistical Association* 47, 260 (1952), 663–685.
- [29] Te-Yuan Huang, Nikhil Handigol, Brandon Heller, Nick McKeown, and Ramesh Johari. 2012. Confused, timid, and unstable: picking a video streaming rate is hard. In *Proceedings of the 2012 internet measurement conference*. 225–238.
- [30] Te-Yuan Huang, Ramesh Johari, Nick McKeown, Matthew Trunnell, and Mark Watson. 2014. A Buffer-Based Approach to Rate Adaptation: Evidence from a Large Video Streaming Service. In *Proceedings of the 2014 ACM Conference on SIGCOMM (SIGCOMM '14)*. Association for Computing Machinery, New York, NY, USA, 187–198. <https://doi.org/10.1145/2619239.2626296>
- [31] Guido W Imbens. 2004. Nonparametric estimation of average treatment effects under exogeneity: A review. *Review of Economics and statistics* 86, 1 (2004), 4–29.
- [32] Junchen Jiang, Vyas Sekar, Henry Milner, Davis Shepherd, Ion Stoica, and Hui Zhang. 2016. {CFA}: A practical prediction system for video qoe optimization. In *13th {USENIX} Symposium on Networked Systems Design and Implementation ({NSDI} 16)*. 137–150.
- [33] Junchen Jiang, Vyas Sekar, Ion Stoica, and Hui Zhang. 2017. Unleashing the potential of data-driven networking. In *International Conference on Communication Systems and Networks*. Springer, 110–126.
- [34] Junchen Jiang, Vyas Sekar, and Hui Zhang. 2012. Improving fairness, efficiency, and stability in http-based adaptive video streaming with festive. In *Proceedings of the 8th international conference on Emerging networking experiments and technologies*. 97–108.
- [35] Maryia Kabanava, Holger Rauhut, and Ulrich Terstiege. 2015. On the minimal number of measurements in low-rank matrix recovery. In *2015 International Conference on Sampling Theory and Applications (SampTA)*. 382–386. <https://doi.org/10.1109/SAMP.2015.7148917>
- [36] Diederik P Kingma and Jimmy Ba. 2014. Adam: A method for stochastic optimization. *arXiv preprint arXiv:1412.6980* (2014).
- [37] S Shunmuga Krishnan and Ramesh K Sitaraman. 2013. Video stream quality impacts viewer behavior: inferring causality using quasi-experimental designs. *IEEE/ACM Transactions on Networking* 21, 6 (2013), 2001–2014.
- [38] Anukool Lakhina, Mark Crovella, and Christophe Diot. 2004. Diagnosing network-wide traffic anomalies. *ACM SIGCOMM computer communication review* 34, 4 (2004), 219–230.
- [39] Anukool Lakhina, Konstantina Papagiannaki, Mark Crovella, Christophe Diot, Eric D. Kolaczyk, and Nina Taft. 2004. Structural Analysis of Network Traffic Flows. *SIGMETRICS Perform. Eval. Rev.* 32, 1 (jun 2004), 61–72. <https://doi.org/10.1145/1012888.1005697>
- [40] Bob Lantz, Brandon Heller, and Nick McKeown. 2010. A network in a laptop: rapid prototyping for software-defined networks. In *Proceedings of the 9th ACM SIGCOMM Workshop on Hot Topics in Networks*. 1–6.
- [41] Mathias Lecuyer, Joshua Lockerman, Lamont Nelson, Siddhartha Sen, Amit Sharma, and Aleksandrs Slivkins. 2017. Harvesting randomness to optimize distributed systems. In *Proceedings of the 16th ACM Workshop on Hot Topics in Networks*. 178–184.
- [42] Yongjun Liao, Wei Du, Pierre Geurts, and Guy Leduc. 2013. DMFSGD: A Decentralized Matrix Factorization Algorithm for Network Distance Prediction. *IEEE/ACM Trans. Netw.* 21, 5 (oct 2013), 1511–1524. <https://doi.org/10.1109/TNET.2012.2228881>
- [43] Greg Linden, Brent Smith, and Jeremy York. 2003. Amazon.com recommendations: Item-to-item collaborative filtering. *IEEE Internet computing* 7, 1 (2003), 76–80.
- [44] Dong Lu, Yi Qiao, P.A. Dinda, and F.E. Bustamante. 2005. Characterizing and Predicting TCP Throughput on the Wide Area Network. In *25th IEEE International Conference on Distributed Computing Systems (ICDCS'05)*. 414–424. <https://doi.org/10.1109/ICDCS.2005.17>
- [45] Hongzi Mao, Mohammad Alizadeh, Ishai Menache, and Srikanth Kandula. 2016. Resource Management with Deep Reinforcement Learning. In *Proceedings of the 15th ACM Workshop on Hot Topics in Networks (HotNets '16)*. Association for Computing Machinery, New York, NY, USA, 50–56. <https://doi.org/10.1145/3005745.3005750>
- [46] Hongzi Mao, Ravi Netravali, and Mohammad Alizadeh. 2017. Neural adaptive video streaming with pensieve. In *Proceedings of the Conference of the ACM Special Interest Group on Data Communication*. 197–210.
- [47] Hongzi Mao, Malte Schwarzkopf, Shaileshh Bojja Venkatakrisnan, Zili Meng, and Mohammad Alizadeh. 2019. Learning Scheduling Algorithms for Data Processing Clusters. In *Proceedings of the ACM Special Interest Group on Data Communication (SIGCOMM '19)*. Association for Computing Machinery, New York, NY, USA, 270–288. <https://doi.org/10.1145/3341302.3342080>
- [48] Yun Mao, Lawrence K. Saul, and Jonathan M. Smith. 2006. IDES: An Internet Distance Estimation Service for Large Networks. *IEEE Journal on Selected Areas in Communications* 24, 12 (2006), 2273–2284. <https://doi.org/10.1109/JSAC.2006.8842026>
- [49] Emily Marx, Francis Y. Yan, and Keith Winstein. 2020. Implementing BOLA-BASIC on Puffer: Lessons for the use of SSIM in ABR logic. (2020). [arXiv:cs.NI/2011.09611](https://arxiv.org/abs/2011.09611)
- [50] Cross-Disorder Group of the Psychiatric Genomics Consortium et al. 2013. Identification of risk loci with shared effects on five major psychiatric disorders: a genome-wide analysis. *The Lancet* 381, 9875 (2013), 1371–1379.
- [51] Adam Paszke, Sam Gross, Francisco Massa, Adam Lerer, James Bradbury, Gregory Chanan, Trevor Killeen, Zeming Lin, Natalia Gimelshein, Luca Antiga, et al. 2019. Pytorch: An imperative style, high-performance deep learning library. *Advances in neural information processing systems* 32 (2019), 8026–8037.
- [52] Judea Pearl. 2009. *Causality: Models, Reasoning and Inference* (2nd ed.). Cambridge University Press, USA.
- [53] Jonas Peters, Dominik Janzing, and Bernhard Schölkopf. 2017. *Elements of causal inference: foundations and learning algorithms*. The MIT Press.
- [54] James M Robins, Miguel Angel Hernan, and Babette Brumback. 2000. Marginal structural models and causal inference in epidemiology. (2000).
- [55] Matthew Roughan, Yin Zhang, Walter Willinger, and Lili Qiu. 2012. Spatio-Temporal Compressive Sensing and Internet Traffic Matrices (Extended Version). *IEEE/ACM Transactions on Networking* 20, 3 (2012), 662–676. <https://doi.org/10.1109/TNET.2011.2169424>
- [56] Donald B Rubin. 2005. Causal inference using potential outcomes: Design, modeling, decisions. *J. Amer. Statist. Assoc.* 100, 469 (2005), 322–331.
- [57] Yossi Rubner, Carlo Tomasi, and Leonidas J Guibas. 1998. A metric for distributions with applications to image databases. In *Sixth International Conference on Computer Vision (IEEE Cat. No. 98CH36271)*. IEEE, 59–66.
- [58] Kevin Spiteri, Rahul Uргаonkar, and Ramesh K. Sitaraman. 2020. BOLA: Near-Optimal Bitrate Adaptation for Online Videos. *IEEE/ACM Transactions on Networking* 28, 4 (2020), 1698–1711.



- <https://doi.org/10.1109/TNET.2020.2996964>
- [59] Panchapakesan C Sruthi, Sanjay Rao, and Bruno Ribeiro. 2020. Pitfalls of data-driven networking: A case study of latent causal confounders in video streaming. In *Proceedings of the Workshop on Network Meets AI & ML*. 42–47.
- [60] Yi Sun, Xiaoqi Yin, Junchen Jiang, Vyas Sekar, Fuyuan Lin, Nanshu Wang, Tao Liu, and Bruno Sinopoli. 2016. CS2P: Improving Video Bitrate Selection and Adaptation with Data-Driven Throughput Prediction. In *Proceedings of the 2016 ACM SIGCOMM Conference (SIGCOMM '16)*. Association for Computing Machinery, New York, NY, USA, 272–285. <https://doi.org/10.1145/2934872.2934898>
- [61] Liying Tang and Mark Crovella. 2003. Virtual Landmarks for the Internet. In *Proceedings of the 3rd ACM SIGCOMM Conference on Internet Measurement (IMC '03)*. Association for Computing Machinery, New York, NY, USA, 143–152. <https://doi.org/10.1145/948205.948223>
- [62] Mukarram Tariq, Amgad Zeitoun, Vytautas Valancius, Nick Feamster, and Mostafa Ammar. 2008. Answering what-if deployment and configuration questions with wise. In *Proceedings of the ACM SIGCOMM 2008 conference on Data communication*. 99–110.
- [63] Eric Tzeng, Judy Hoffman, Kate Saenko, and Trevor Darrell. 2017. Adversarial discriminative domain adaptation. In *Proceedings of the IEEE conference on computer vision and pattern recognition*. 7167–7176.
- [64] Madeleine Udell and Alex Townsend. 2019. Why are big data matrices approximately low rank? *SIAM Journal on Mathematics of Data Science* 1, 1 (2019), 144–160.
- [65] Francis Y. Yan, Hudson Ayers, Chenzhi Zhu, Sadjad Fouladi, James Hong, Keyi Zhang, Philip Levis, and Keith Winstein. 2020. Learning in situ: a randomized experiment in video streaming. In *17th USENIX Symposium on Networked Systems Design and Implementation (NSDI 20)*. USENIX Association, Santa Clara, CA, 495–511. <https://www.usenix.org/conference/nsdi20/presentation/yan>
- [66] Yuzhe Yang, Guo Zhang, Dina Katabi, and Zhi Xu. 2019. Me-net: Towards effective adversarial robustness with matrix estimation. *arXiv preprint arXiv:1905.11971* (2019).
- [67] Xiaoqi Yin, Abhishek Jindal, Vyas Sekar, and Bruno Sinopoli. 2015. A Control-Theoretic Approach for Dynamic Adaptive Video Streaming over HTTP. *SIGCOMM Comput. Commun. Rev.* 45, 4 (Aug. 2015), 325–338. <https://doi.org/10.1145/2829988.2787486>
- [68] Dong Zhang, Hanwang Zhang, Jinhui Tang, Xiansheng Hua, and Qianru Sun. 2020. Causal intervention for weakly-supervised semantic segmentation. *arXiv preprint arXiv:2009.12547* (2020).
- [69] Qizhen Zhang, Kelvin K. W. Ng, Charles Kazer, Shen Yan, João Sedoc, and Vincent Liu. 2021. MimicNet: Fast Performance Estimates for Data Center Networks with Machine Learning. In *Proceedings of the 2021 ACM SIGCOMM 2021 Conference (SIGCOMM '21)*. Association for Computing Machinery, New York, NY, USA, 287–304. <https://doi.org/10.1145/3452296.3472926>

## APPENDIX A TENSOR COMPLETION WITH POLICY INVARIANCE

Here, we discuss a more generic version of the problem considered in §4 from the lens of tensor completion. Specifically, in Section 4 we considered simplified setting where the observed mediator were considered to be of one dimensional. Here, we shall consider higher dimensional observed mediator. This, naturally suggests using the lens of Tensor instead of Matrix completion. We will also discuss how higher dimensional observed mediator can enable recovery of more complex system dynamics or model compared to the simple solution we discussed in Section 4 for rank 1 setup.

**Potential Outcomes Tensor.** As considered in Section 4 let all possible actions be denoted as  $[A] = \{1, \dots, A\}$  for some  $A \geq 2$ . Let the observed mediator be of  $D$  dimension. As before, we have  $N$  traces or trajectories of interest with trace or trajectory  $i \in [N]$  being of length  $H_i \geq 1$  time steps. As before, let  $U = \sum_{i=1}^N H_i$ .

Consider an order-3 tensor  $M$  of dimension  $A \times U \times D$ , where  $M = [m_{\alpha\beta\gamma} : \alpha \in [A], \beta \in [U], \gamma \in [D]]$  with  $m_{\alpha\beta\gamma}$  corresponds to the  $\gamma$ th co-ordinate of the  $D$ -dimensional mediator corresponding to action  $a_t = \alpha \in [A]$  when exogenous latent state is  $u_{i,t}$  with  $\beta$  corresponding to enumeration of  $(i,t)$  for some  $i \in [N]$  and  $t \leq H_i$ . Recall that, as explained in Section 4, all possible  $(i,t) : t \leq H_i, i \in [N]$  are mapped to an integer in  $[U]$ . We call this tensor  $M$  as the Potential Outcomes Tensor.

Indeed, if we know  $M$  completely, then we can answer the task of simulation or counterfactual estimation well since we will be able to estimate the mediator for each trajectory under a given possible sequence of counterfactual actions, and subsequently estimate the counterfactual observation (assuming we could learn the  $\mathcal{F}_{\text{systems}}$ ).

We shall assume that there are  $P \geq 1$  policies under which these traces were observed. In particular, each trajectory was observed under one of these  $P$  policies and the assignment of policy to the trajectory was done uniformly at random. Define  $\Pi_p \subset [U]$  as collection of indices corresponding to trajectories  $i \in [N]$  and their times  $t \leq H_i$  where trajectory  $i$  was assigned policy  $p$  for  $p \in [P]$ . Let  $U_p = |\Pi_p|$ .

**Tensor factorization, low CP-rank.** The tensor  $M$  admits (not necessarily unique) factorization of the form: for any  $\alpha \in [A], \beta \in [U], \gamma \in [D]$

$$m_{\alpha\beta\gamma} = \sum_{\ell=1}^r x_{\alpha\ell} y_{\beta\ell} z_{\gamma\ell}, \quad (9)$$

for some  $r \geq 1$ . For any tensor, such a factorization exists with  $r$  at most  $\text{poly}(A, U, D)$ .

*Assumption 1 (low-rank).* We shall make an assumption that  $r$  is *small*, i.e. does not scale with  $A, U, D$  and specifically a small constant.

*Assumption 2 (sufficient measurements).* We shall assume that number of measurements per instance,  $D$ , is at least as large as the underlying rank  $r$  of the tensor  $M$ , i.e.  $D \geq r$ .

**Distributional invariance and RCT.** As before, we shall assume that the distribution of exogenous latent states is invariant across policies due to random assignment of policies to trajectories in the setup of RCT. In the context of the tensor  $M$ , this corresponds to the distribution invariance of factors  $y_\beta \in \mathbb{R}^r$  over  $\beta \in \Pi_p$  for any  $p \in [P]$ . Concretely, for any  $p \neq p' \in [P]$  and  $\ell \in [r]$ , we have

$$\frac{1}{U_p} \sum_{\beta \in \Pi_p} y_{\beta\ell} \approx \frac{1}{U_{p'}} \sum_{\beta' \in \Pi_{p'}} y_{\beta'\ell}. \quad (10)$$

More generally, any finite moment (not just first moment or average) of exogenous latent states should be empirically invariant across policies. As in Section 4, we would like to utilize property (10) to estimate the tensor  $M$ .

**A Simple Estimation Method and When It Works.** We describe a simple method that can recover entire tensor as long as rank  $r \leq D$ . For simplicity, we shall assume  $r = D$  (the largest possible rank for which method will work). By (9), for a given fixed  $\alpha \in [A]$  and across  $\beta \in [U], \gamma \in [D]$ ,

$$m_{\alpha\beta\gamma} = \sum_{\ell=1}^r y_{\beta\ell} \tilde{z}_{\gamma\ell}^\alpha, \quad (11)$$

where  $\tilde{z}_{\gamma\ell}^\alpha = x_{\alpha\ell} z_{\gamma\ell}$ . Since  $D = r$ , the matrix  $\tilde{Z}^\alpha = [\tilde{z}_{\gamma\ell}^\alpha : \gamma \in [D], \ell \in [r]]$  is a square matrix. With this notation, we have that for any fixed  $\alpha \in [A]$ , the matrix  $M^\alpha = [m_{\alpha\beta\gamma} : \beta \in [U], \gamma \in [D]] \in \mathbb{R}^{U \times D}$  (or  $\mathbb{R}^{U \times r}$  since  $r = D$ ) can be represented as

$$M^\alpha = Y \tilde{Z}^{\alpha,T}, \quad (12)$$

where  $Y = [y_{\beta\ell} : \beta \in [U], \ell \in [r]] \in \mathbb{R}^{U \times r}$ .

*Assumption 3 (full rank).* We shall assume that the  $D \times D$  (i.e.  $r \times r$ ) square matrices  $\tilde{Z}^\alpha$  for each  $\alpha \in [A]$  are full rank and hence invertible.

The *Assumption 3* implies that  $Y = M^\alpha (\tilde{Z}^{\alpha,T})^{-1}$  for all  $\alpha \in [A]$ .

For policy  $p \in [P]$ , indices  $\beta \in \Pi_p$  are relevant. For a given  $\beta \in \Pi_p$ , if the policy  $p$  utilized action  $\alpha \in [A]$ ,  $m_{\alpha\beta} \in \mathbb{R}^D$  is observed. To that end, let  $\Pi_{p,\alpha} = \{\beta \in \Pi_p : \text{policy utilized action } \alpha\}$ . Let  $U_{p,\alpha} = |\Pi_{p,\alpha}|$  for any  $\alpha \in [A]$ . Then, define  $Y^{p,\alpha} = [y_{\beta\ell} : \beta \in \Pi_{p,\alpha}, \ell \in [r]] \in \mathbb{R}^{U_{p,\alpha} \times r}$ ,  $M^{\alpha,p} = [m_{\alpha\beta\gamma} : \beta \in \Pi_{p,\alpha}, \gamma \in [D]]$ . Then we have  $Y^{p,\alpha} = M^{\alpha,p} (\tilde{Z}^{\alpha,T})^{-1}$ .

Therefore, for any  $\ell \in [r=D]$ ,

$$\begin{aligned} \sum_{\beta \in \Pi_{p,\alpha}} y_{\beta\ell} &= \mathbf{1}^{p,\alpha,T} Y^p \mathbf{e}_\ell \\ &= \mathbf{1}^{p,\alpha,T} M^{\alpha,p} (\tilde{Z}^{\alpha,T})^{-1} \mathbf{e}_\ell, \end{aligned} \quad (13)$$

where  $\mathbf{1}^{p,\alpha} \in \mathbb{R}^{U_{p,\alpha}}$  is vector of all 1s, and  $\mathbf{e}_\ell \in \mathbb{R}^r$  be vector with all entries 0 but the  $\ell \in [r]$ th co-ordinate 1.

Then, for any  $\ell \in [r]$  and  $p \in [P]$ ,

$$\begin{aligned} \frac{1}{U_p} \sum_{\beta \in \Pi_p} y_{\beta\ell} &= \frac{1}{U_p} \sum_{\beta \in \Pi_{p,\alpha}} y_{\beta\ell} \\ &= \frac{1}{U_p} \sum_{\alpha \in [A]} \sum_{\beta \in \Pi_{p,\alpha}} \mathbf{1}^{p,\alpha,T} M^{\alpha,p} (\tilde{Z}^{\alpha,T})^{-1} \mathbf{e}_\ell \\ &= \sum_{\alpha \in [A]} \left( \frac{1}{U_p} \sum_{\beta \in \Pi_{p,\alpha}} \mathbf{1}^{p,\alpha,T} M^{\alpha,p} \right) (\tilde{Z}^{\alpha,T})^{-1} \mathbf{e}_\ell \\ &= \sum_{\alpha \in [A]} M^{\alpha,p} (\tilde{Z}^{\alpha,T})^{-1} \mathbf{e}_\ell, \end{aligned} \quad (14)$$

where  $M^{\alpha,p} = \left( \frac{1}{U_p} \sum_{\beta \in \Pi_{p,\alpha}} \mathbf{1}^{p,\alpha,T} M^{\alpha,p} \right) \in \mathbb{R}^{1 \times r}$  is an observed quantity, while  $\tilde{Z}^{\alpha,T}$  is unknown. Using (14) and (10), we obtain that for any  $\ell \in [r]$  and  $p \neq p' \in [P]$ ,

$$\sum_{\alpha \in [A]} M^{\alpha,p} (\tilde{Z}^{\alpha,T})^{-1} \mathbf{e}_\ell \approx \sum_{\alpha \in [A]} M^{\alpha,p'} (\tilde{Z}^{\alpha,T})^{-1} \mathbf{e}_\ell. \quad (15)$$

Let  $\tilde{z}^{\alpha,\ell} = (\tilde{Z}^{\alpha,T})^{-1} \mathbf{e}_\ell \in \mathbb{R}^r$  be the  $\ell$ th column vector of  $r \times r$  matrix  $(\tilde{Z}^{\alpha,T})^{-1}$ . Then (15) implies that for any  $\ell \in [r]$  and  $p \neq p' \in [P]$ ,

$$\sum_{\alpha \in [A]} (M^{\alpha,p} - M^{\alpha,p'}) \tilde{z}^{\alpha,\ell} \approx 0. \quad (16)$$

Thinking of a flattened vector  $\mathbf{z} \in \mathbb{R}^{Ar^2}$  obtained by concatenating  $r$ -dimensional vectors  $\tilde{z}^{\alpha,\ell}$  across  $\alpha \in [A]$  and  $\ell \in [r]$ , (16) can be re-written as, for any  $p \neq p' \in [P]$ ,

$$\mathbf{v}^{p,p',T} \mathbf{z} \approx 0, \quad (17)$$

where  $\mathbf{v}^{p,p'} \in \mathbb{R}^{Ar^2}$  is vector formed using entries from  $M^{\alpha,p} - M^{\alpha,p'}$  across  $\alpha \in [A]$  and stacking them up appropriately. By definition,  $\mathbf{v}^{p,p'}$  is observed quantity for each  $p \neq p' \in [P]$ . Now if we consider  $P-1$  equations produced by considering pair of policies (1,2),(2,3),..., $(P-1,P)$  in (17), by design they are non-redundant linear equations. Let matrix  $\mathbf{V} \in \mathbb{R}^{(P-1) \times Ar^2}$  be formed by stacking  $\mathbf{v}^{1,2}, \dots, \mathbf{v}^{P-1,P}$ .

*Assumption 4 (policy requirements).* Let  $P \geq Ar^2 + 1$  and the rank of  $\mathbf{V} = Ar^2 - 1$ .

Under Assumption 4, it follows that we can uniquely (upto scaling) recover  $\mathbf{z}$  by solving for system of linear equation  $\mathbf{Vz} = \mathbf{0}$  as the null space of  $\mathbf{V}$  is of dimension 1.

Once we know  $\mathbf{z}$ , i.e. by undoing flattening, we obtain  $(\tilde{Z}^{\alpha,T})^{-1}$  for each  $\alpha \in [A]$ . Since for each policy  $p \in [P]$  and

$\alpha \in [A]$ ,  $Y^{p,\alpha} = M^{\alpha,p} (\tilde{Z}^{\alpha,T})^{-1}$  and we observe  $M^{\alpha,p}$ , we can recover  $Y^{p,\alpha}$  and hence subsequently  $Y \in \mathbb{R}^{U \times r}$ .

By (12), we can now recover slice of tensor  $M$ , the  $M^\alpha$  for each  $\alpha \in [A]$ , and hence we can recover entire tensor  $M$  as desired.

## APPENDIX B CAUSALSIM'S ALGORITHM

Algorithm 1 provides a detailed description of CausalSim's training procedure.

---

### Algorithm 1 CausalSim Training

---

- 1: initialize  $g_\psi$  to represent the action encoder
  - 2: initialize  $\mathcal{E}_\theta$  to represent the latent factor extractor
  - 3: initialize  $\Phi_\zeta$  to represent the function  $\Phi$
  - 4: initialize  $\mathcal{P}_\varphi$  to represent  $\mathcal{F}_{\text{system}}$
  - 5: initialize  $\mathcal{W}_\gamma$  to represent the *policy discriminator*
  - 6: initialize hyper-parameters  $\kappa, \delta$
  - 7: initialize batch size  $b$
  - 8: initialize learning rates  $\eta_1, \eta_2, \eta_3, \eta_4, \eta_5$
  - 9: initialize hyper-parameter  $\text{num\_train\_it}, \text{num\_disc\_it}$
  - 10: initialize dataset  $D \leftarrow \{(o_i, m_i, a_i, \pi_i)\}_{i=1}^m$  from an RCT
  - 11: **for**  $\text{num\_train\_it}$  **do**
  - 12:     **for**  $\text{num\_disc\_it}$  **do**
  - 13:         sample batch  $B \leftarrow \{(o_l, m_l, a_l, \pi_l)\}_{l=1}^b$
  - 14:         **for**  $l=1, 2, \dots, b$  **do**
  - 15:              $u_l \leftarrow \mathcal{E}_\theta(m_l, a_l)$
  - 16:             **end for**
  - 17:              $\gamma = \gamma - \eta_1 \cdot \nabla_\gamma \left[ \frac{-1}{b} \sum_{l=1}^b \log \mathcal{W}_\gamma(\pi_l | \hat{u}_l) \right]$
  - 18:             **end for**
  - 19:         sample batch  $B \leftarrow \{(o_{l+1}, o_l, m_l, a_l, \pi_l)\}_{l=1}^b$
  - 20:         **for**  $l=1, 2, \dots, b$  **do**
  - 21:              $u_l \leftarrow \mathcal{E}_\theta(m_l, a_l)$
  - 22:              $\hat{m}_l \leftarrow \Phi_\zeta(g_\eta(a_l), u_l)$
  - 23:             **end for**
  - 24:              $\mathcal{L}_{\text{disc}} \leftarrow \frac{-1}{b} \sum_{l=1}^b \log \mathcal{W}_\gamma(\pi_l | u_l)$
  - 25:              $\mathcal{L}_{\text{pred}} \leftarrow \frac{1}{b} \sum_{l=1}^b (o_{l+1} - \mathcal{P}_\varphi(o_l, a_l, \hat{m}_l))^2 + \delta (m_l - \hat{m}_l)^2$
  - 26:              $\mathcal{L}_{\text{total}} \leftarrow \mathcal{L}_{\text{pred}} - \kappa \times \mathcal{L}_{\text{disc}}$
  - 27:              $\psi = \psi - \eta_2 \cdot \nabla_\psi \mathcal{L}_{\text{pred}}$
  - 28:              $\theta = \theta - \eta_3 \cdot \nabla_\theta \mathcal{L}_{\text{total}}$
  - 29:              $\zeta = \zeta - \eta_4 \cdot \nabla_\zeta \mathcal{L}_{\text{pred}}$
  - 30:              $\varphi = \varphi - \eta_5 \cdot \nabla_\varphi \mathcal{L}_{\text{pred}}$
  - 31:         **end for**
-

## APPENDIX C REAL-WORLD ABR

### C.1 Comprehensive results

Figure 8 compares CausalSim predictions with ExpertSim and SLSim baselines in all possible source/left-out policy pairs.

### C.2 What makes a simulation scenario easy/hard?

Figure 8 shows source, target, and simulated buffer level distributions in all possible source/target scenarios of the Puffer dataset. In about 30% of these scenarios, which we call *easy* scenarios, all simulators perform well. However, in about 70% of the source/target scenarios, which we call *hard* simulation scenarios, baseline predictions are highly biased towards the source distributions. In these hard scenarios, CausalSim is able to de-bias the trajectories and its predictions match target distribution pretty well. So it is natural to wonder what makes a simulation scenario easy/hard?

An easy simulation scenario happens when source and target policies take similar actions. Similar action means that the factual achieved throughput (of the source policy) is similar to the counterfactual achieved throughput (of the target policy). This is what both ExpertSim (explicitly) and SLSim (implicitly) assume for doing simulation. Making this assumption is the core reason their simulations are biased in hard cases, where source and target policies take different actions, as we discussed in detail in §2.1.3.

Figure 9 validates our reasoning for difficulty of a simulation scenario. X axis shows the mean absolute difference between source and simulation actions (bitrates) when simulating with SLSim in a specific source/target scenario. Y axis shows EMD (Our performance metric for simulation, smaller is better) of both baselines in that specific scenario.

Two main cluster of points are clearly visible in this figure. The pink cluster on the bottom left corresponds to easy simulations. It includes all source/target simulation scenarios where baselines perform well (bottom), and at the same time, source and target actions are quite similar (left).

The green cluster on the top right corresponds to the hard simulations. It includes all source/target simulation scenarios where baselines fail to perform an unbiased simulation (top), and at the same time, source and target actions are quite different (right).

### C.3 Can we do a More Fine-grained Evaluation?

Ideally, we would like to evaluate CausalSim’s counterfactual predictions on a step-by-step basis for a given trajectory. But as discussed in §6.1.1, this is not possible in real-world data, as we only see the outcome of one ABR algorithm’s chosen action for a single step. In other words, there is no way to get

ground truth for individual counterfactual predictions in the observational data, which is referred to as the fundamental problem of Causal Inference[27]. This is the reason we evaluated predictions on a distributional level.

However, there is a way to evaluate CausalSim’s predictions at a more fine-grained level. Instead of evaluating the predicted distribution of buffer occupancy across the whole population, we can evaluate on certain *sub-populations* of users. The only requirement is that the way we select these sub-populations should be statistically independent of the ABR algorithm. For example, we can partition users by a metric such as Min RTT, which is independent of the policy chosen for each user in the RCT. Min RTT is an inherent property of a network path<sup>9</sup>, and we would expect Min RTT distribution to be the same for users assigned to different ABR policies.

We use the MinRTT to create the following four sub-populations:

- (1) Sub1: users with  $\text{Min RTT} < 35^{ms}$
- (2) Sub2: users with  $35^{ms} \leq \text{Min RTT} < 70^{ms}$
- (3) Sub3: users with  $70^{ms} \leq \text{Min RTT} < 100^{ms}$
- (4) Sub4: users with  $100^{ms} \leq \text{Min RTT}$

Now, we can ask question of the following type: *had the users in sub-population two, who were assigned the source ABR algorithm, instead used the left-out ABR algorithm, what would the distribution of their buffer level look like?* As the ground truth answer to this question, we can use the buffer level distribution of users in sub-population two assigned to the left-out policy.

Figure 10b shows the CDF of CausalSim’s EMD when simulating the left-out ABR algorithm over the whole population, and each of the above sub-populations. We can see that the EMD achieved for sub-populations is similar to the whole population, indicating that CausalSim’s predictions are good across all sub-populations. This further suggests that even at surgically small subpopulations, CausalSim maintains accuracy, and does not overfit to whole distribution.

### C.4 How to Tune CausalSim’s Hyper-parameters?

Counterfactual prediction is not a standard supervised learning task that optimizes in-distribution generalization. Rather, it is always an OOD generalization problem, i.e., we collect data from a training policy (distribution 1), and want to accurately simulate data under a different policy (distribution 2). Since we do not use data from the test policy when we train CausalSim, we use the following natural proxy for tuning hyper-parameters: *Simulating ABR algorithms in the training data using trajectories of other ABR algorithms in the training data*. This of course can be viewed as an OOD problem as

<sup>9</sup>This is true to a first order approximation, if we ignore the possibility that a video streaming session drives up queueing delays throughout the course of a video, thereby inflating the observed Min RTT.

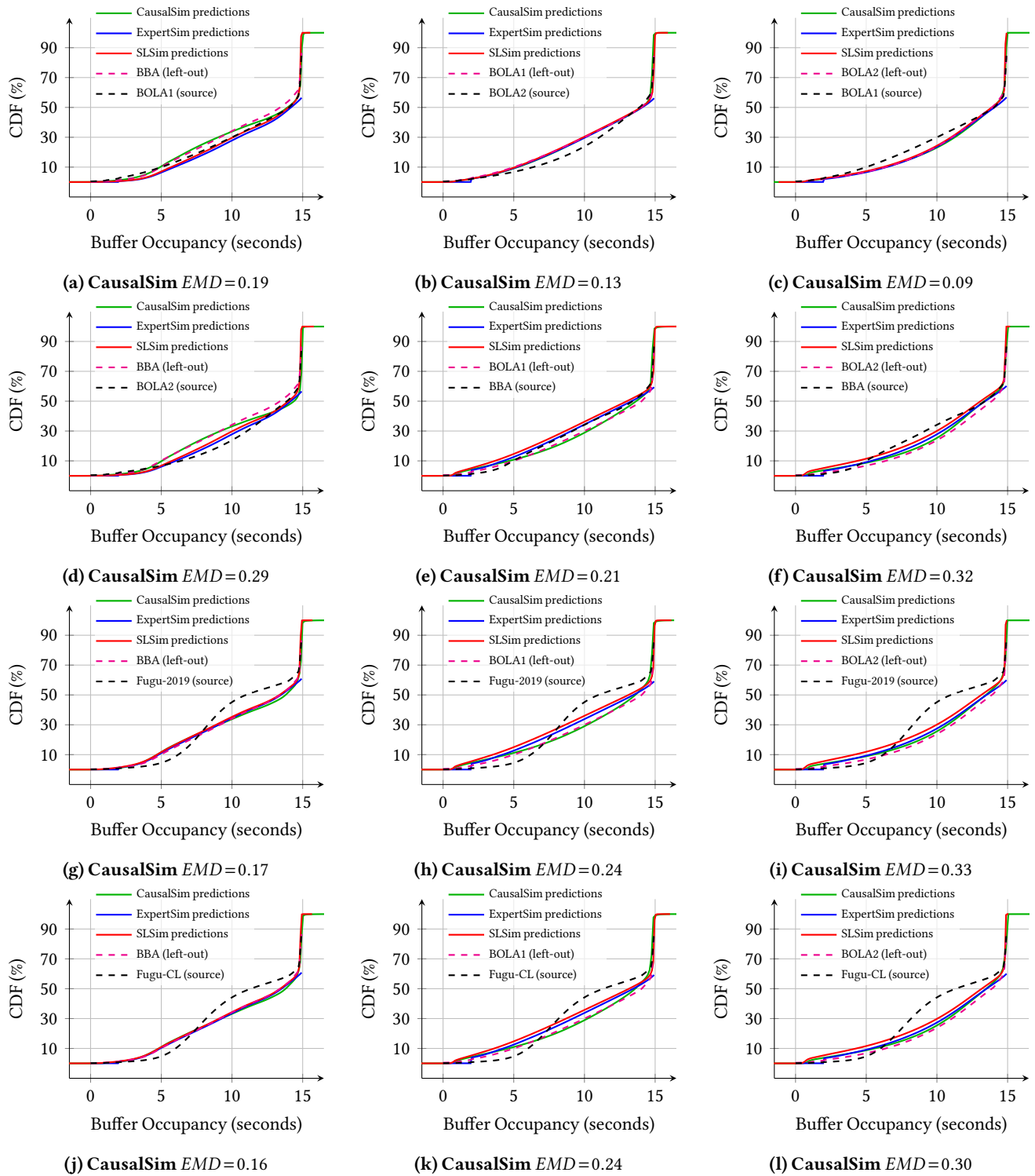
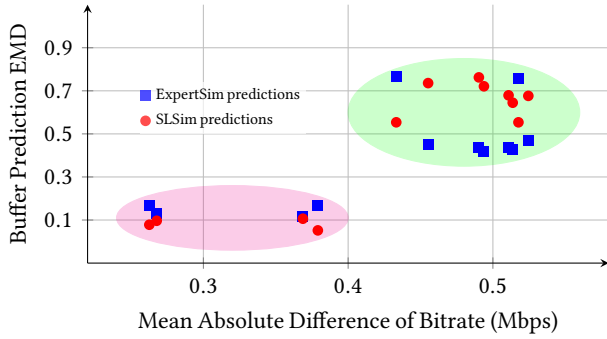


Figure 8: Buffer level distribution of source, target, CausalSim predictions, and baseline predictions across all source/target scenarios.



**Figure 9: Simulation difficulty is related to how different counterfactual actions are from factual ones. This figure shows scatterplot of EMD versus mean absolute bitrate difference, for ExpertSim and SLSim, over all possible source left-out pairs. The pink cluster signifies the ‘easy’ scenarios and the green cluster signifies ‘hard’ ones.**

well. We claim that if a choice of hyper-parameters results in a robust model that performs well OOD across all validation ABR algorithms in the training data, it should work well for the actual left-out test policy as well.

We verify this hyper-parameter tuning procedure empirically. For each choice of the three left-out ABR algorithms (hence training dataset), we train six different CausalSim models with different choices of  $\kappa$  (defined in (8)). We consider two metrics: (i) *Test EMD*, defined as the average EMD when simulating the left-out ABR algorithm from the ABR algorithms in the training data. This is our main performance objective. (ii) *Validation EMD*, defined as the average EMD when simulating ABR algorithms in the training dataset from other ABR algorithms in the training dataset. This is our proxy objective for hyper-parameter tuning.

For each model (18 in all: 3 datasets, 6 hyper-parameters), we calculate both Test EMD and Validation EMD, which results in one (Validation EMD, Test EMD) point in Figure 10a. The PCC between Valid EMD and Test EMD is 0.94, which shows high linear correlation. Hence, though CausalSim might not always perform well (i.e., Test EMD is not low for some combinations of training dataset and hyper-parameters), we can have a very good idea of how well it works by measuring Validation EMD.

### C.5 Dataset & Algorithms

Our trajectories in the real-world (Puffer) data come from the time span of August 1, 2020 until May 15, 2021. In this period of time, 5 ABR algorithms appear consistently and are listed in Table 1. Each trajectory is an active client session streaming a live TV channel. We used trajectories with a minimum length

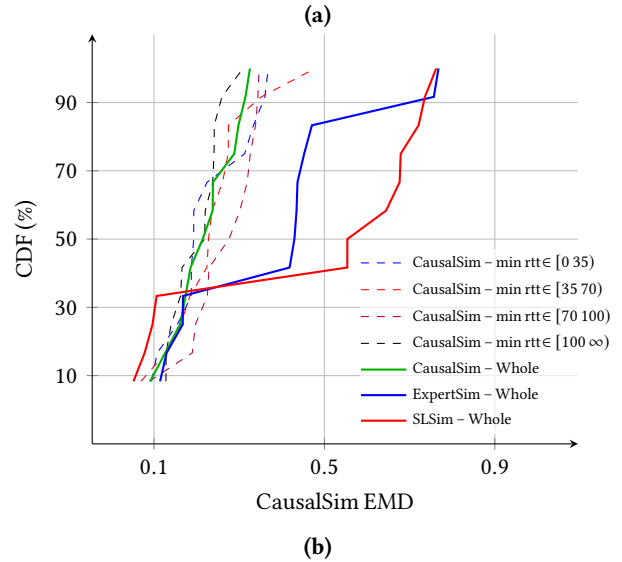
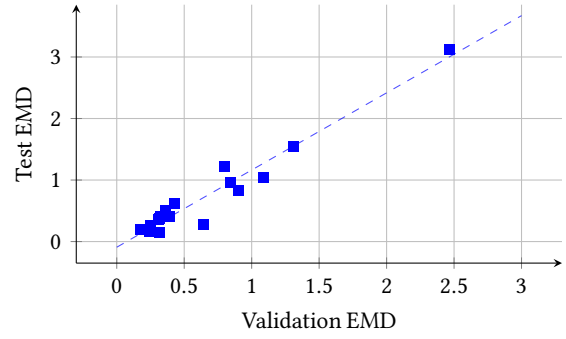


**Figure 10: Top: validation EMD and test EMD are highly correlated. This justifies our hyper-parameter tuning strategy. Bottom: Comparing the distribution of CausalSim EMDs in the whole population with smaller sub-populations with ExpertSim and SLSim.**

of 500 chunks to filter out short-lived sessions. The observed throughputs are in the range of  $200Kbps$  to  $300Mbps$ . Since the highest quality chunks rarely surpass  $7Mbps$ , paths with higher bandwidth will always stream the highest quality chunks under all policies. Hence we only use trajectories with less than  $7Mbps$  of average observed bandwidth.

To test out CausalSim, we need to simulate the streaming session using a different algorithm than the one that was actually used in that session. This requires implementation of the ABR algorithms. However, Fugu’s implementation needs access to the history of the streaming session’s Transmission Control Protocol (TCP) info, which is not fully logged in the data-set. More specifically, our attempts for reconstructing Fugu’s chosen chunk sizes fail to match the logged ones in the data-set. Therefore, we do not consider Fugu-2019 or Fugu-CL as candidates for left-out algorithms.



Policies	Hyperparameter	Value	Used as source	Used as left out
BBA	Cushion	3 (as used in puffer)	✓	✓
	Reservoir	10.5 (as used in puffer)		
BOLA-BASIC v1	$V$	0.67 (As computed in puffer)		
	$\gamma$	-0.43 (As computed in puffer)	✓	✓
	Utility function	$\log_{10}(1 - ssim)$ (As used in puffer)		
	Minimum utility	0 (As used in puffer)		
	Maximum utility	60 (As used in puffer)		
	$V$	51.4 (As computed in puffer)		
BOLA-BASIC v2	$\gamma$	-0.43 (As computed in puffer)	✓	✓
	Utility function	$ssim$ (As used in puffer)		
	Minimum utility	0 (As used in puffer)		
	Maximum utility	1 (As used in puffer)		
Fugu-CL	-	-	✓	×
Fugu-2019	-	-	✓	×

Table 1: ABR algorithms used in the real-world dataset and experiments

## C.6 Training setup

We use MLPs as the neural network structures for CausalSim models and the SLSim model. All implementations use the Pytorch [51] library. Table 2 is a comprehensive list of all hyperparameters used in training.

## APPENDIX D SYNTHETIC ABR

As explained in §6.1.2, we also evaluate CausalSim in a synthetic ABR environment, in which we can obtain ground truth for individual counterfactual predictions on a step-by-step basis for a trajectory. In these experiments, we also use a larger set of policies than available in the real data.

### D.1 Simulation Dynamics

In each simulated training session, we start with an empty playback buffer and a latent network path characterized by an RTT and a capacity trace. In each step, an ABR algorithm chooses a chunk size, which is transported over this network path to the client as the buffer is depleting. Once the user receives the chunk, the buffer level increases by the chunk duration. This simple system can be modeled as follows:

$$b_{t+1} = \min(b_t - d_t, 0) + c \quad (18)$$

where  $b_t$ ,  $d_t$  and  $c$  refer to the buffer level at time step  $t$ , the download time of the chunk at time step  $t$ , and the chunk video length in seconds, respectively. Streaming the

next chunk is started immediately following receiving the previous one, except when the buffer level surpasses a certain value (in our case, 10 seconds to mimic a live-stream ABR setting). To compute  $d_t$ , we model the transport as a TCP session with an Additive Increase - Multiplicative Decrease (AIMD) congestion control mechanism with slow start. For every chunk, the TCP connection starts from the minimum window size of 2 packets and increases the window according to slow start. Therefore, it takes the transport some time to begin fully utilizing the available network capacity. The overhead incurred by slow start depends on the RTT and bandwidth-delay product of the path. When downloading chunks with large sizes, the probing overhead is minimal but it can be significant for small chunks. Therefore, as we observed in the Puffer data, the throughput achieved for a given chunk in this synthetic simulation depends on the size of the chunk.

Our simulation consists of 5000 to 16000 trajectories, for each of whom a policy is randomly chosen from the list of available policies. For a full explanation of the simulation setup, network capacity generation procedure, and the simulated policies, refer to §D.4.

**Performance Metric:** We compare CausalSim predictions with ground truth counterfactual trajectories, via the Mean Squared Error (MSE) distance between the two time series:

$$MSE(\mathbf{p}, \mathbf{q}) = \|\mathbf{p} - \mathbf{q}\|_2^2 \quad (19)$$

Model	Hyperparameter	Value
SLSim (1 network), CausalSim (3 networks)	Hidden layers	(128, 128)
	Hidden layer Activation function	Rectified Linear Unit (ReLU)
	Output layer Activation function	Identity mapping
	Optimizer	Adam [36]
	Learning rate	0.001
	$\beta_1$	0.9
	$\beta_2$	0.999
	$\epsilon$	$10^{-8}$
	Batch size	$2^{19}$
	CausalSim	$\kappa$
$\delta$		{0}
Training iterations (num_train_it)		5000
num_disc_it		10
SLSim		Training iterations

Table 2: Training setup and hyperparameters for the real-world ABR experiment

Here,  $\mathbf{p} = \{p_t\}_{t=1}^N$  and  $\mathbf{q} = \{q_t\}_{t=1}^N$  are time series vectors. Better predictions yield smaller MSE values, where an ideal MSE is 0.

## D.2 Low-rank structure

As discussed in §4.1, we can formulate the counterfactual estimation problem in the context of matrix completion. For each time step, we know the chosen bitrate (action) and the achieved throughput (mediator). We also know the mediator is computed using a latent factor and the action. Suppose the latent factor is the network bottleneck capacity  $c_t$ <sup>10</sup>.  $\mathcal{F}_{\text{mediation}}$  describes how the achieved throughput (the mediator) relates to this latent factor. Intuitively, this should be a close-to-linear function,  $m_t \approx c_t$ . But it’s not exactly linear; for example, congestion control may under-utilize the network capacity for small transfers on high-RTT paths.

We form a matrix  $M$ , where the rows denote actions  $a_t \in [A]$  and the columns denote the latent factors  $u_t^i$  for each trajectory. The ‘factual’ data we have are single observed mediator values in each column, i.e for each step and each latent, we have observed the mediator from a single action. To estimate counterfactuals, we must complete the matrix. This modeling inherently assumes low-rank structure  $M$ , which results from  $\mathcal{F}_{\text{mediation}}$ . However, we have no way of knowing the true  $\mathcal{F}_{\text{mediation}}$  in the Puffer dataset. But to get a sense for what it might look like and whether it’s plausible that  $M$  is

low rank, we can investigate this in a simple controlled ABR environment which confirms the low-rank assumption.

Let us consider a simple model of congestion control that allows us to compute the observed throughput. We describe this model in detail in §D.1, but the basic idea is to assume that for each chunk, the congestion control begins in slow start and ramps up its window size over several RTTs until it fills up the available capacity or the transfer completes. For this model,  $\mathcal{F}_{\text{mediation}}$  takes the following form:

$$\text{Let } \hat{RTT} := \frac{RTT}{\ln(2)}$$

$$m_t = \begin{cases} \frac{c_t}{1 + \frac{\hat{RTT} \cdot (\ln(c_t/\dot{c}) - c + \dot{c})}{s_t}} & \text{if } s_t \geq \hat{RTT} \cdot (c_t - \dot{c}) \\ \frac{s_t}{\hat{RTT} \cdot \ln(\frac{s_t}{\hat{RTT} \cdot \dot{c}} + 1)} & \text{otherwise} \end{cases} \quad (20)$$

where  $s_t$  is the chunk size (which itself is determined by the bitrate chosen by ABR) and  $\dot{c}$  is the starting download rate in the slow start algorithm (in our case, equal to 2 MTUs). We use this model to generate a version of  $M$  with  $A=6$  actions and  $U=49000$  latent network conditions. We compute the singular value decomposition with the 6 singular values represented in non-increasing order ( $\sigma_1 \geq \sigma_2 \geq \dots \geq \sigma_6$ ). The total ‘energy’ of matrix is given by sum of squares of these singular values. It turns out that  $\frac{\sigma_1^2 + \sigma_2^2}{\text{total energy}}$  is more than 0.999. This suggests that most of the matrix is captured by its rank-2

<sup>10</sup>There may be other latent factors but bottleneck capacity is likely to have the strongest influence on the achieved throughput.

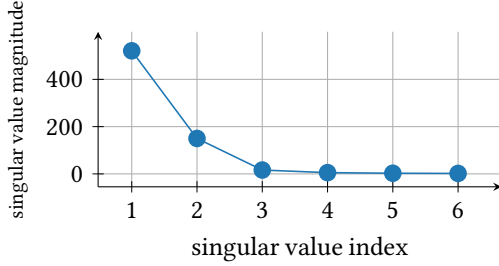


**Figure 11: Singular values of potential outcome matrix  $M$  associated with synthetic ABR suggest that  $M$  is approximately rank 2.**

approximation, as depicted in fig. 11. In other words,  $M$  is approximately low ( $=2$ ) rank.

### D.3 Can CausalSim Faithfully Simulate New Policies?

Similar to our real-data evaluations, we train models based on training data generated using all policies except a left-out policy, for which the model does not observe any data. Although traces come from the same generative process, no two trajectories in the dataset collected with different policies share the exact same trace, as this would be an unrealistic data collection scenario. Given that we have 9 possible policies to leave out, we have 9 possible datasets and models. There are 8 possible groups of trajectories to choose as sources, based on the policy that generated them. In total this leaves 72 different combinations and scenarios. We use the same hyper-parameter tuning approach examined in §C.4. Figure 12a compares the CDF of MSE values resulting from CausalSim and the two baselines. As evident, both baselines suffer from inaccurate predictions and in some cases are catastrophically inaccurate. On the contrary, CausalSim maintains favorable performance, even in the tail of its MSE distribution. Figure 12b gives a closer look at the CDF curves. We see CausalSim dominates at every scale.

Figure 12c is a heatmap of the two dimensional histogram of CausalSim predictions and ground truths. A fully accurate prediction scheme would perfectly match the ground truth and only the diagonal of this histogram would be populated. CausalSim almost achieves that, indicating it produces accurate trajectories on a step-by-step basis.

Further, in Figure 13, we compare the the Mean Absolute Percentage Error (MAPE) of CausalSim, ExpertSim and SLSim predictions across all trajectories at each time step for the first 35 steps. Note that the error naturally accumulates for all three methods as we move forward in time. However, CausalSim maintains a MAPE of ( $\sim 5.1\%$ ) which significantly lower than both ExpertSim’s and SLSim’s ( $\sim 10\%$ ).

### D.4 Data & Algorithms

Simulating a trajectory in our synthetic ABR environment needs three components:

- A video, with several bit-rates available. We use "Envivio-Dash3" from the DASH-246 JavaScript reference client [19].
- An ABR algorithm. We have a set of 9 policies to choose from, presented in Table 3.
- A network path, which is characterized by the latent network capacity and the path RTT.

We use random generative processes to generate network traces and RTTs. The RTT for a streaming session is sampled randomly, according to a uniform distribution:

$$rtt \sim Unif(10\text{ ms}, 500\text{ ms})$$

Our trace generator is a bounded Gaussian distribution, whose mean comes from a Markov chain. Prior work shows Markov chains are appropriate models for TCP throughput [60], and Gaussian distributions can model throughputs in stationary segments of TCP flows [44].

Concretely, at the start of the trace, the following parameters are randomly sampled:

$$\begin{aligned} v &\sim Unif(30, 100) \\ p &= 1/v \\ l, h &\sim Unif(0.5, 4.5) \\ \text{s.t. } \frac{h-l}{h+l} &> 0.3 \\ s_0 &\sim Unif(l, h) \\ c_\sigma &\sim Unif(0.05, 0.3) \end{aligned}$$

At each time step, the state remains unchanged with probability  $1-p$  and changes otherwise. When changing, the next state is sampled from a double exponential distribution centered around the previous state:

$$\begin{aligned} \lambda &= solve(1 - e^{h-s_{t-1}} - e^{s_{t-1}-l} = 0) \\ s_t &= DoubleExp(s_{t-1}, \lambda) \end{aligned}$$

The point for this specific transition kernel is that small changes in network capacity should be more likely than drastic changes. Finally, the network capacity  $c_t$  in each step is sampled from a Gaussian distribution, defined by these parameters:

$$c_t \sim Normal(s_t, s_t \cdot c_\sigma)$$

### D.5 Training setup

Similar to the real-world ABR experiment, we use MLPs as the neural network structures for CausalSim models and the SLSim model. Table 4 comprehensively lists all hyperparameters used in training.

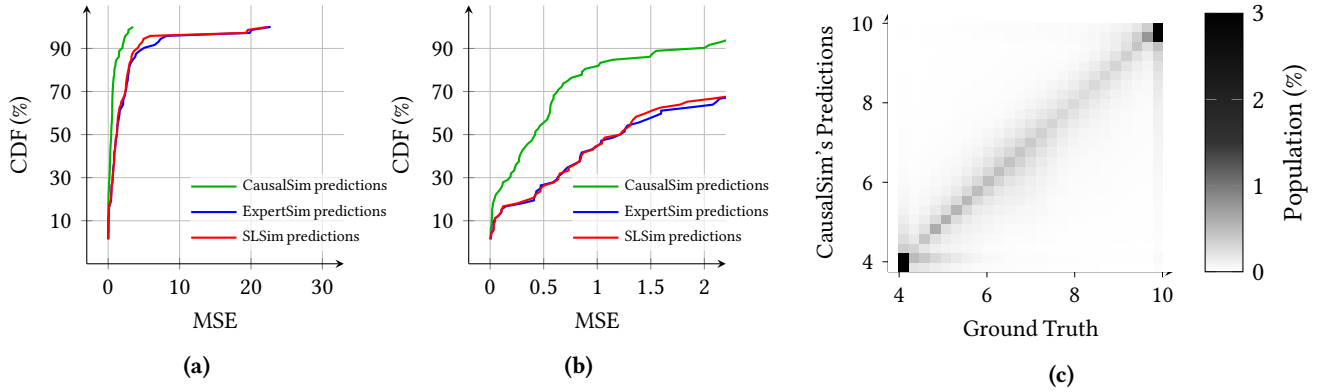


Figure 12: *Left*: Distribution of CausalSim, ExpertSim, and SLSim MSEs over all possible source left-out pairs. *Middle*: The same figure with a smaller MSE range. In a this magnified view, CausalSim clearly outperforms the baselines. *Right*: Two-dimensional histogram heatmap of CausalSim predictions vs. ground truth.

Policies	Hyperparameter	Value	Used as source	Used as left out
<b>BBA</b>	Cushion	5	✓	✓
	Reservoir	10		
<b>BOLA-BASIC</b>	$V$	0.71 (Computed using puffer formula)	✓	✓
	$\gamma$	0.22 (Computed using puffer formula)		
	Utility function	$\ln(\text{chunk sizes})$ (As used in BOLA paper[58])		
<b>Random</b>	-	-	✓	✓
<b>BBA-Random mixture 1</b>	Cushion	5	✓	✓
	Reservoir	10		
	Random choices	50%		
<b>BBA-Random mixture 2</b>	Cushion	10	✓	✓
	Reservoir	20		
	Random choices	50%		
<b>MPC</b>	Lookback length	5	✓	✓
	Lookahead length	5		
	Rebuffer penalty	4.3		
	Throughput estimate	Harmonic mean		
<b>Rate-based</b>	Lookback length	5	✓	✓
	Throughput estimate	Harmonic mean		
<b>Optimistic Rate-based</b>	Lookback length	5	✓	✓
	Throughput estimate	Max		
<b>Pessimistic Rate-based</b>	Lookback length	5	✓	✓
	Throughput estimate	Min		

Table 3: ABR algorithms used in the synthetic ABR experiments.

Model	Hyperparameter	Value
CausalSim (4 networks)	Hidden layers (SLSim)	(128, 128)
	Hidden layers (CausalSim: Extractor, Discriminator and $\mathcal{F}_{system}$ )	(128, 128)
	Hidden layers (CausalSim: Action encoder)	(64, 64)
	Rank $r$	2
	Hidden layer Activation function	ReLU
	Output layer Activation function	Identity mapping
	Optimizer	Adam [36]
SLSim (1 network)	Learning rate	0.0001
	$\beta_1$	0.9
	$\beta_2$	0.999
	$\epsilon$	$10^{-8}$
	Batch size	$2^{13}$
CausalSim	$\kappa$	{0.01, 0.1, 1, 10, 100}
	$\delta$	{0, 1}
	Training iterations (num_train_it)	20000
	num_disc_it	10
SLSim	Training iterations	20000

Table 4: Training setup and hyperparameters for the synthetic ABR experiments.

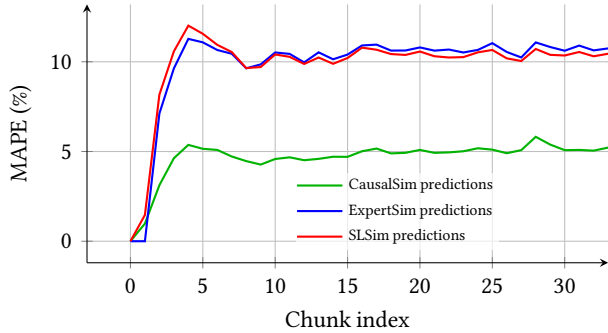


Figure 13: A time series plot of the Mean Absolute Percentage Error (MAPE) across all trajectories, for CausalSim, ExpertSim and SLSim predictions. Notice how errors can aggregate in trajectory simulation.

## D.6 RL setup

We use the A2C algorithm for training the policies. Table 5 lists all hyperparameters for the RL training.

## APPENDIX E LOAD BALANCING

### E.1 Data & Algorithms

To simulate the load balancing problem described in §6.3.1, we need to set the server processing rates  $\{r_i\}_{i=1}^N$ , and arriving

job sizes  $S_k$ . Server rates are generated randomly, as follows:

$$r_i = e^{u_i}$$

where  $u_i \sim \text{Unif}(-\ln(5), \ln(5))$

We generate job sizes using a time-varying Gaussian distribution. At step  $k$  of the trajectory, job size  $S_k$  is sampled as follows:

$$S_k \sim \text{Normal}(\mu_k, \sigma_k)$$

where  $\mu_k$  and  $\sigma_k$  signify the mean and variance of the generative distribution at time step  $k$ . At each time step, with a probability of  $p = 1/12000$ , the mean and variance change and with a probability of  $1 - p$ , they remain the same. The mean and variance values are drawn from random distributions, both at the start of a trajectory and when a change occurs, in the following manner:

If  $k=0$  (start of trace) or, mean and variance must change:

$$\mu_k \sim \text{Pareto}(\alpha=1, L=10^1, H=10^{2.5})$$

$$\sigma_k \sim \text{Unif}(0, 0.5\mu_k)$$

Else:

$$\mu_k = \mu_{k-1}$$

$$\sigma_k = \sigma_{k-1}$$

Group	Hyperparameter	Value
Neural Network	Hidden layers	(32, 32)
	Hidden layer activation function	ReLU
	Output layer activation function	A2C actor: Softmax A2C critic: Identity mapping
	Optimizer	Adam [36]
	Learning rate	0.001
	$\beta_1$	0.9
	$\beta_2$	0.999
	$\epsilon$	$10^{-8}$
	Weight decay	$10^{-4}$
A2C training	Episode lengths	490
	Epochs to convergence ( $T_c$ )	8000 (3920000 samples)
	Random seeds	4
	$\gamma$	0.96
	Entropy schedule	0.1 to 0 in 5000 epochs
	$\lambda$ (for GAE)	0.95
Environment	Chunk length $c$	4
	Number of actions (bitrates)	6

**Table 5: Training setup and hyperparameters for learning RL policies in the synthetic ABR environment.**

Policies	Description	Used as source	Used as left out
Server limited policy (8 variations)	Randomly assign to only two servers	✓	✗
Shortest queue	Assign to server with smallest queue	✓	✓
Power of $k$ ( $k \in \{2,3,4,5\}$ )	Poll queue lengths of $k$ server and assign to shortest queue	✓	✓
Oracle optimal	Normalize queue sizes with server rates and assign to shortest normalized queue	✓	✓
Tracker optimal	Similar to oracle, but estimates server rates with historical observations of processing times	✓	✓

**Table 6: Scheduling policies used in the load balancing experiment.**

Jobs generated according to this process are temporally correlated, and therefore not independent and identically distributed. Training data consists of 5000 trajectories of length 1000, each of which was randomly assigned a policy from Table 6.

Finally, Table 6 describes the 16 policies used in these experiments.

## E.2 Training setup

As before, we use MLP as the neural network structures for CausalSim models and the SLSim model and Table 5 is a comprehensive list of all hyperparameters used in training. Note

that, as mentioned in §6.3, we assume access to  $\mathcal{F}_{\text{system}}$  and focus on the more challenging task of estimating the mediator quantities, for both CausalSim and SLSim. Therefore, in training, there are no observations and hence  $\mathcal{L}_{\text{total}}$  consist of only two terms: the squared loss of the mediator quantities and the discriminator loss. Given this, we only use one value for the hyper-parameter  $\delta$ , which we set to one.



<b>Model</b>	<b>Hyperparameter</b>	<b>Value</b>	
<b>CausalSim</b> (3 networks)	Hidden layers (SLSim)	(128, 128)	
	Hidden layers (CausalSim: Extractor, Discriminator)	(128, 128)	
	Hidden layers (CausalSim: Action encoder)	No hidden layers	
	Rank $r$	1	
	Hidden layer Activation function	ReLU	
	Output layer Activation function	Identity mapping	
	Optimizer	Adam [36]	
	<b>SLSim</b> (1 network)	Learning rate	0.0001
		$\beta_1$	0.9
		$\beta_2$	0.999
$\epsilon$		$10^{-8}$	
Batch size		$2^{13}$	
<b>CausalSim</b>	$\kappa$	{0.01, 0.1, 1, 10, 100}	
	$\delta$	{1}	
	Training iterations (num_train_it)	10000	
	num_disc_it	10	
<b>SLSim</b>	Training iterations	10000	

**Table 7: Training setup and hyperparameters for the load balancing experiment.**